A Comprehensive Genetic Characterization of Bacterial Motility

Hany S. Girgis[1,2], Yirchung Liu[1,2], William S. Ryu[1], Saeed Tavazoie[1,2*]

1 Lewis-Sigler Institute for Integrative Genomics, Princeton University, Princeton, New Jersey, United States of America, **2** Department of Molecular Biology, Princeton University, Princeton, New Jersey, United States of America

We have developed a powerful experimental framework that combines competitive selection and microarray-based genetic footprinting to comprehensively reveal the genetic basis of bacterial behaviors. Application of this method to *Escherichia coli* motility identifies 95% of the known flagellar and chemotaxis genes, and reveals three dozen novel loci that, to varying degrees and through diverse mechanisms, affect motility. To probe the network context in which these genes function, we developed a method that uncovers genome-wide epistatic interactions through comprehensive analyses of double-mutant phenotypes. This allows us to place the novel genes within the context of signaling and regulatory networks, including the Rcs phosphorelay pathway and the cyclic di-GMP second-messenger system. This unifying framework enables sensitive and comprehensive genetic characterization of complex behaviors across the microbial biosphere.

Citation: Girgis HS, Liu Y, Ryu WS, Tavazoie S (2007) A comprehensive genetic characterization of bacterial motility. PLoS Genet 3(9): e154. doi:10.1371/journal.pgen.0030154

Introduction

Structured microbial habitats have selected for a dazzling diversity of bacterial behaviors. These behaviors are contingent on sophisticated sensory systems that maximize fitness in the complex and highly dynamic environments where physical, chemical, and biological parameters change on many different time scales. Modern genetic and molecular studies have largely focused on a limited repertoire of behaviors of a few model organisms in the non-native context of the laboratory. However, even at the level of basic phenomenology, the vast majority of phenotypes in the microbial biosphere remain uncharacterized. A major challenge of the post-genome era is the development of efficient and comprehensive methods for revealing the genetic basis of these behaviors across diverse clades, especially as the emerging field of metagenomics begins to reveal the wide assortment of microbial life on the planet [1].

Chemotaxis, the capacity to move up and down chemical gradients, is widespread in the bacterial world. An impressive achievement of 20th-century biology was a systems-level understanding of bacterial chemotaxis in terms of the structures, interactions, and organization of the roughly 50 constituent molecular components [2–4]. The best-characterized chemotaxis machineries are those of *E. coli* and its close relative *Salmonella enterica* [5,6]. These species propel themselves by rotating multiple extracellular helical filaments called flagella. When the filament rotates in the counterclockwise (CCW) direction, as viewed from outside the cell, a helical wave travels down the filament away from the cell body. In this CCW mode, multiple rotating flagella come together to form a bundle, propelling the cell forward in a motion called "smooth swimming." When one or more motors reverse to the clockwise (CW) direction, the bundle comes apart and the cell "tumbles" briefly, reorienting the cell in a new direction; subsequent motor switching to the CCW direction causes the cell to swim forward again. The direction of rotation is influenced by the output of the chemotaxis network, which consists of a signal transduction cascade that allows robust adaptation to local concentrations of ligands over many orders of magnitude [7,8]. When cells detect an increase in the concentration of an attractant, tumbling is suppressed so as to allow cells to migrate towards the source through the statistical strategy of a biased random walk [9]. The signaling circuit that mediates this behavior terminates at the flagellar machinery, which is synthesized through a sequential hierarchy of gene activation events [10] initiated by the expression of the master transcriptional regulator FlhDC. These events yield an orderly "just-in-time" expression and assembly of the flagellar components [11], which consist of a basal body complex and a filament. The basal body complex contains a central rod that connects the motor to the filament through a short hook.

The identification of the molecular components and their organization into the two dominant modules—the chemotaxis network and the flagellum/basal body/motor system—took the better part of 40 years and the work of dozens of laboratories. These efforts have culminated in a level of understanding nearly unmatched in any other domain of molecular biology. For these reasons, flagellar-mediated motility is an ideal test case for any modern post-genomic approach that attempts to efficiently and comprehensively reveal the genetic basis of a complex bacterial phenotype. In this study, we make improvements on a microarray-based genetic footprinting strategy [12], increasing its sensitivity and specificity in revealing the

Editor: David S. Guttman, University of Toronto, Canada

Received June 7, 2007; **Accepted** July 25, 2007; **Published** September 14, 2007

A previous version of this article appeared as an Early Online Release on July 25, 2007 (doi:10.1371/journal.pgen.0030154.eor).

Abbreviations: CCW, counterclockwise; c-di-GMP, cyclic di-GMP; CW, clockwise; DGC, diguanylate cyclase; LPS, lipopolysaccharides; OPG, osmoregulated periplasmic glucans; ORF, open reading frame; PDE, phosphodiesterase; PFU, plaque-forming unit

* To whom correspondence should be addressed. E-mail: tavazoie@molbio.princeton.edu

Author Summary

Bacteria thrive in a limitless range of extreme environments, accompanied by exotic metabolisms and sophisticated behaviors. However, our modern molecular understanding of bacteria comes from studies of a limited range of phenotypes in a handful of model organisms such as *E. coli* and *Bacillus subtilis*. With the availability of thousands of sequenced bacterial genomes, there is now an urgent need for methods that rapidly and comprehensively reveal the genetic basis of phenotypes across the microbial biosphere. To this end, we have developed a genome-wide experimental framework that quantifies the degree to which every gene in the genome contributes to a phenotype of interest, and reveals the organization of genes within regulatory networks and signaling pathways. We show here that the application of this methodology to *E. coli* swimming and surface motility reveals essentially all the previously known components of flagellar-mediated chemotaxis on the time scale of weeks. Remarkably, we also identify three dozen additional novel loci that operate through diverse mechanisms to affect a behavior that was assumed to be completely characterized. The speed, ease, and broad applicability of this framework should greatly accelerate the global analysis of a wide range of uncharacterized bacterial behaviors.

contribution of each and every gene in the genome to a phenotype of interest. We demonstrate the manner in which this strategy can be used to explore the genetic basis of complex bacterial behavior by following the population dynamics of *E. coli* insertional mutants in environments where reproductive fitness is coupled to motility. To fully identify the genetic determinants for this phenotype, a library of transposon-mutagenized cells was functionally enriched en masse for impaired swimming and surface-mediated swarming motility. We also selected for resistance to bacteriophage χ, which is known to infect and lyse cells only when they are motile. Additionally, we identified the genetic basis of motility suppression by environmental factors. Using DNA microarray hybridization, we monitored the relative abundance of each mutant throughout the selections. The comprehensive nature of our methodology is reflected by the identification of nearly all of the known structural and regulatory components of flagellar-mediated chemotaxis. Strikingly, we also identify dozens of additional loci that contribute to this phenotype. Further characterization of these novel genes revealed that they impair motility through diverse mechanisms such as disrupting signaling through phosphorelay cascades, altering concentrations of the recently appreciated cyclic di-GMP (c-di-GMP) second messenger, and by mechanisms that have yet to be revealed. Subsequent genome-wide epistasis analyses allow us to organize the discovered loci into signaling and regulatory pathways. This systematic framework for genetic characterization can be applied to any microorganism that is amenable to transposon mutagenesis, making it accessible to the vast majority of bacterial systems of importance to basic, industrial, environmental, and clinical research.

Results/Discussion

Mapping Phenotype to Genotype Using Microarray-Based Genetic Footprinting

Traditional methods of genetic investigation have been extremely successful in providing a deep molecular understanding of many phenotypes in model microorganisms. However, faced with literally thousands of important and mostly uncharacterized bacterial species, we need entirely novel methods of genetic functional analysis and pathway elucidation that scale to the task at hand. In this study, we have applied a systematic genome-wide strategy to determine the contribution of nearly all genetic loci in the genome to a phenotype of interest. Our approach combines genetic footprinting [13] with microarray hybridization [14] in order to monitor, in parallel, the relative abundances of transposon-mutagenized cells throughout a competitive selection experiment [12]. Saturation transposon mutagenesis is a powerful, versatile, and efficient strategy for creating comprehensive mutant libraries for genomic functional characterization [15]. We have used a hyperactive Tn5 transposition system with reduced target specificity [16] to create a library of approximately 5×10^5 independent transposon insertional mutants in *E. coli* MG1655. Given the reduced target specificity and a genome of approximately 4,300 genes, the mutagenesis of our library is saturating with an average of ~100 independent insertions within each open reading frame (ORF).

In each of our experiments, a population of mutants is challenged for competitive growth under a selection of interest. Each mutant within the population is uniquely defined by the local sequence flanking the transposon insertion site. The series of molecular manipulations detailed in Figure S1 allow the amplification of roughly 200 base pairs flanking each transposon insertion site in a population in parallel. Fluorescent labeling and hybridization of the amplicons to a spotted DNA microarray (created as described in Protocol S1) reveal the relative abundance of each mutant as reflected by the signal intensity of the corresponding ORF on the array. As a consequence of selection, individual insertional mutants can increase or decrease in abundance during the course of an experiment, and these relative changes can be monitored by comparing genome-wide hybridization values before and after selection. In a proof-of-principle analysis of the unselected transposon library, we show that the hybridization intensities corresponding to known essential genes are strongly biased towards the lowest values, consistent with their inability to harbor transposon insertions (Figure S2).

Quantitative Analysis of Selection within the Pool of Mutants

To determine the degree to which each gene contributes to fitness under a particular selection, we quantify the extent of enrichment or depletion of all transposon insertions within a gene after a selection is imposed. We assign the total hybridization signal for each ORF on the array as the sum of contributions from all the mutants that harbor an insertion somewhere within or in close proximity to the ORF. The ORF intensities from five hybridizations of the maximally diverse unselected library (Dataset S1) are used as a statistical reference to quantify the degree of enrichment or depletion after the library is exposed to a selection of interest. In this way, the five unselected hybridizations define the null variation with respect to which significant differences are quantified. The normalized hybridization intensity value (x) of an ORF from a selection experiment is compared to the null distribution for that ORF (mean: $<x_n>$, standard

deviation: σ), by calculating a *z*-score: $z = (x - \langle x_n \rangle)/\sigma$. ORFs that harbor deleterious mutations during the selection will have negative *z*-scores (corresponding to depletion), whereas ORFs that harbor relatively favorable mutations during the selection will have positive *z*-scores (corresponding to enrichment). In other words, the *z*-score reflects the number of standard deviations above or below the mean of the unselected replicates.

Genetic Basis of Swimming Motility and Chemotaxis

Semi-solid tryptone agar provides a robust setting for studying *E. coli* chemotaxis. Once inoculated into a region of the soft agar, bacteria deplete local nutrients and chemotax radially outward following the concentration gradient of preferred substrates [17]. To systematically and completely identify the genetic determinants for swimming motility, $\sim 10^7$ cells of the mutant library were functionally enriched en masse for an impaired ability to swim through soft agar. After an 8-h incubation to allow motile cells to swim away from the site of inoculation, the population enriched for nonmotile mutants was transferred to a fresh plate for further enrichment (Figure 1A). The percentage of nonmotile mutants was determined after each stage of enrichment by a clonal plating assay and, after five stages, 96% of the mutants showed an impaired ability to swim (Figure S3). The amplification of transposon insertion sites from a small sample of these mutants showed that the nonmotile phenotype is the result of a single gene disruption in each mutant. As expected, the vast majority of these disruptions occurred in previously known flagellar or chemotaxis genes (Table S3). However, even in this small sample, we found transposon insertions in genes without a previously known role in motility.

To obtain a genome-wide catalog of loci involved in swimming motility, we applied our microarray-based genetic footprinting assay to the population of mutants at the end of the enrichments. The *z*-scores reveal that the vast majority of ORFs lie within a tight Gaussian-shaped distribution centered around zero (Figure 1B). However, of the 115 ORFs with *z*-scores greater than 12, 49 are known flagellar and chemotaxis genes. Since the microarray contained 52 out of the total of 54 known motility genes [18], the chance likelihood of observing this level of enrichment was extremely low ($p < 10^{-76}$). The three remaining motility genes that were not significantly enriched are two chemoreceptor genes, *trg* and *aer*, and the filament cap chaperone, *fliT*. Based on the hybridization results, insertional mutations in these genes should not measurably impair motility. We confirmed this expectation by showing that deletions of *fliT* and *aer* did not affect motility (data not shown). The neutral behavior of the *fliT* mutation is not surprising since *fliT* null strains were found to make functional flagella in *S. enterica* [19]. In addition, it has been reported that *fliT* mutations enhance expression of class 2 flagellar operons [20] because FliT acts as a negative regulator of these operons by binding to and inhibiting the activity of FlhDC [21]. The protein encoded by *aer* mediates oxygen and redox sensing, and as such shares overlapping function with the Tsr receptor [22]. Because of this redundancy, only *aer tsr* double mutants are expected to show a motility phenotype in tryptone plates. Finally, the product of *trg* is a transmembrane methyl-accepting chemotaxis protein that senses ribose and galactose [23]. Although these sugars are absent from tryptone plates, deletion of *trg* did result in a measurable motility defect (unpublished data). Therefore, of the more than 50 known genes involved, *trg* is the only false negative under the motility conditions we used.

Remarkably, the selection results revealed many genes with high *z*-scores without a previously known role in motility. We were concerned that some marginally high *z*-scores may be due to "hitchhiking" of spontaneously arising mutations in motility genes on the background of transposon insertions in nonessential genes. To minimize such false positives, we demanded that a candidate motility gene obtain a *z*-score above 12 in at least two of the three replicate selections (Datasets S2, S3, and S4). The 40 candidate genes that fit these criteria were targeted for deletion, and 20 of them were found to show a significant defect in swimming motility (Figure 1C; Table S1). We observed that some false positives were indeed due to hitchhiking, but others were due to polar effects of transposon insertions on downstream genes within operons. Additionally, some genes may be deemed false positive because the nature of the mutation caused by transposon insertion cannot be replicated by a clean deletion of the gene. The criteria we used for identifying candidate motility genes favored sensitivity (essentially 100%) over specificity. However, the number of false positives can be driven lower by decreasing the cycles of selection, increasing the number of replicates, or by focusing on genes with relatively high *z*-scores. In the sections that follow, we explore the manner in which the validated newly identified genes affect motility.

Identifying Flagellar Components through Bacteriophage χ Selection

As a complementary approach to determining the components necessary for a functioning flagellum, we designed a simple selection to identify mutants resistant to χ-phage infection. Bacteriophage χ infects *E. coli* by attaching to and traveling along flagellar filaments [24]. CCW flagellar rotation and the correct pattern of grooves on the surface of the flagellum are thought to drive χ-phage down the filament to the surface of the membrane, very similar to how a nut follows the grooves of a rotating bolt [25]. The library of transposon insertional mutants was exposed to χ-phage in an environment conducive to motility (Figure 2A). Survival of a mutant meant either the loss of its flagella, the loss of flagellar CCW rotation, or the loss of other components necessary for infection. In a sample of mutants taken after selection, 98% were completely nonmotile (Figure S4).

Figure 2B shows the distribution of *z*-scores after library selection upon exposure to bacteriophage χ, and the complete microarray results for duplicate selections can be found in Datasets S5 and S6. As expected, insertional mutations in flagellar genes conferred resistance to χ-phage infection. In contrast, while mutants of the chemotaxis sensory network were in high abundance after the chemotaxis selection, insertional mutants of *cheA, cheB, cheR, cheW, tap, tar, trg,* and *tsr* were in low abundance after exposure to χ-phage. This is to be expected, since null mutations in these genes do not entirely abolish CCW flagellar rotation. The only exception among the *che* genes is *cheZ,* whose *z*-score of +8.7 indicates a CW flagellar rotation bias and reduced susceptibility to χ-phage infection. CheZ is a phosphatase of CheY, the protein whose phosphorylated state biases the flagella

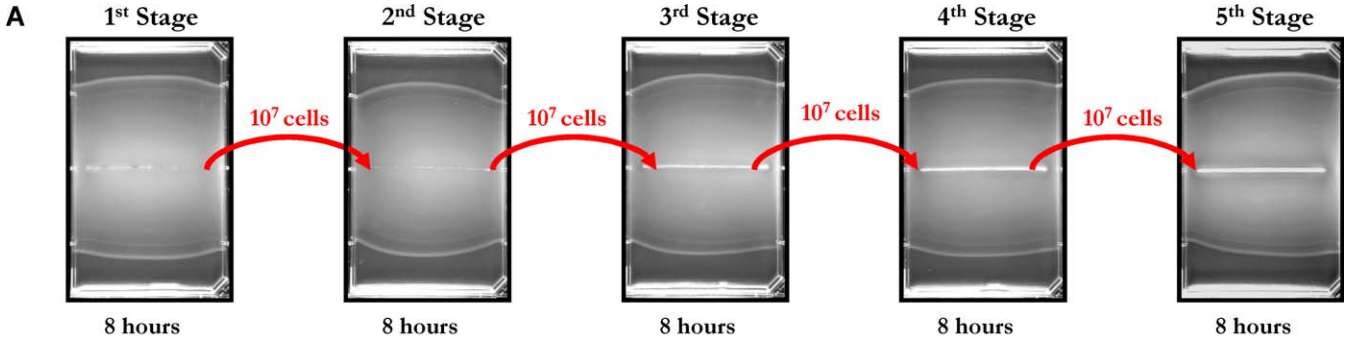

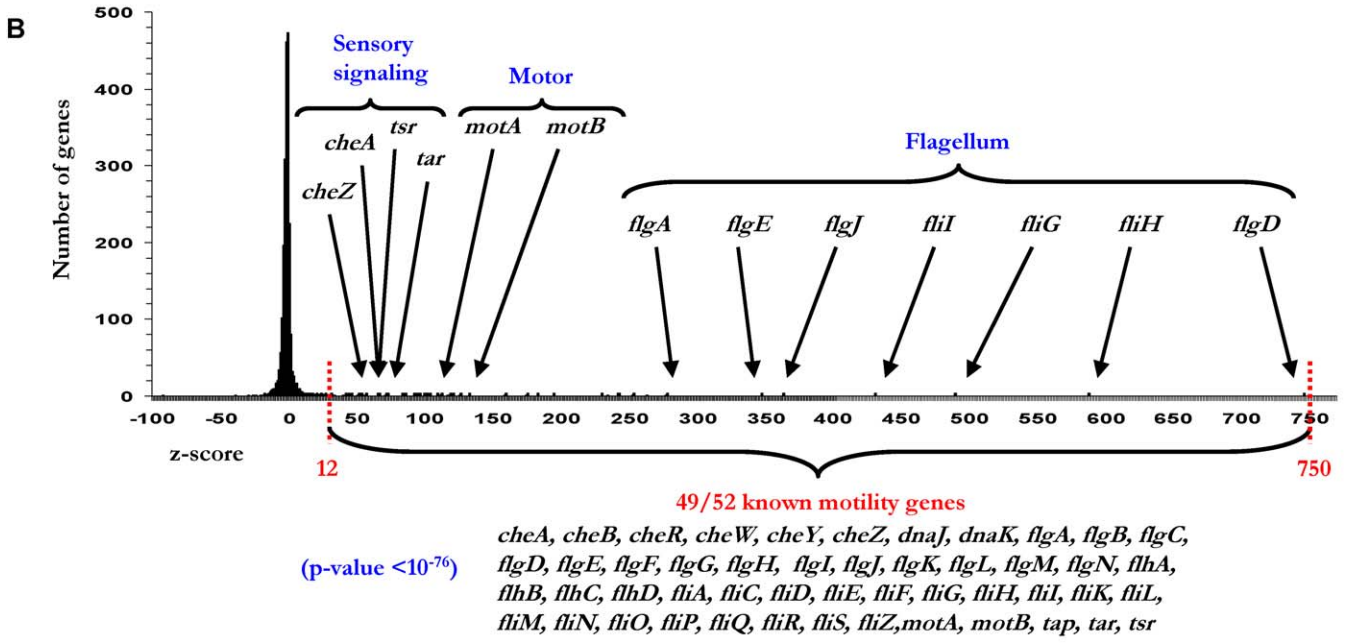

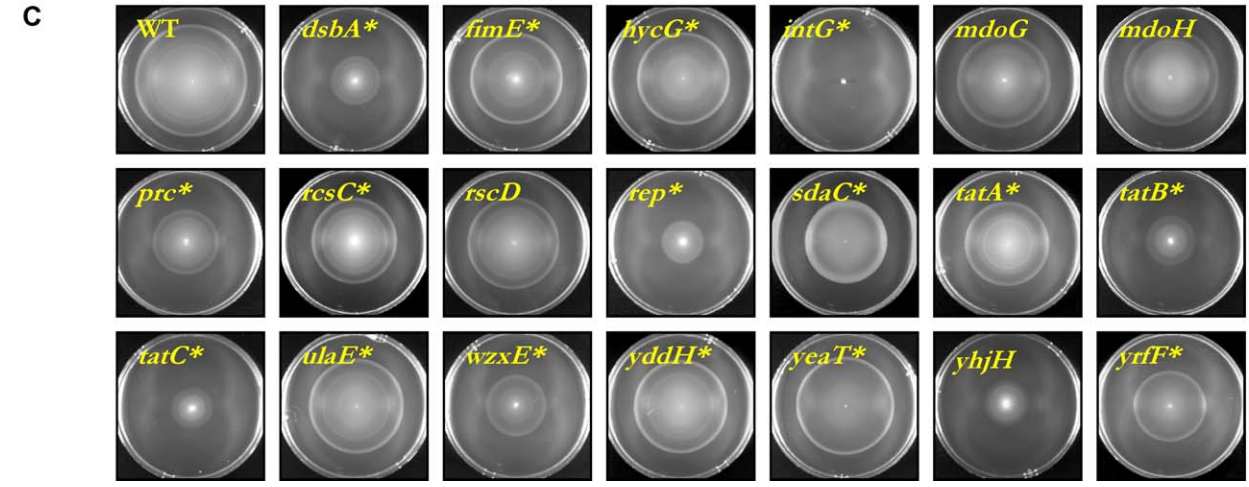

Figure 1. Systematic Identification of Genes Involved in Swimming Motility

(A) Serial enrichment for nonmotile mutants was initiated by inoculating ~10^8 mutants along the center of a soft-agar plate and allowing motile cells to chemotax away. Subsequent stages of enrichment consisted of transferring ~10^7 cells from the original inoculation site to a fresh soft-agar plate. The serial enrichment for nonmotile mutants is reflected by the increasingly dense growth at the site of inoculation.

(B) Genes encoding components of the flagellar and chemotaxis machinery are extremely highly enriched. The vast majority of known flagella and chemotaxis genes (49/52) were identified by hybridization of the pool of mutants after selection for nonmotility. The *z*-scores represent number of standard deviations above or below the mean of the five unselected library replicates.
(C) The swimming phenotype of motility mutants identified through selection and microarray-based genetic footprinting. The null mutations in these genes were introduced by targeted deletion or obtained from an independent library of transposon mutants. These mutants show variable defects in swimming, from severe (*intG*) to mild (*yddH*). Asterisks indicate genes not previously known to affect motility.
doi:10.1371/journal.pgen.0030154.g001

toward the CW direction [26,27]. Therefore, in the absence of CheZ, CheY is maintained in the phosphorylated state, "locking" flagellar rotation in the CW direction, and hence minimizing infection by χ-phage. In addition to these findings, the selection results revealed that cellular structures other than the flagella may be required for infection (Table S1). The role these structures play in χ-phage infection and the impact they have on motility are discussed in a separate section below.

Genetic Basis of Swarming Motility

Whereas flagellar-mediated swimming is among the best-understood bacterial behaviors, very little is known about the genetic program that leads to the development of swarming. Swarming is exhibited by many flagellated bacteria, and is defined as a coordinated multicellular migration across a solid surface by morphologically differentiated cells [28]. Confocal fluorescence microscopy shows swarming cells aligning themselves lengthwise and moving coordinately in groups, forming "rafts" (Movie S1). In this context, the cells appear to execute smooth swimming behavior almost exclusively, in contrast to the extensive switching back and forth seen during chemotaxis. Aside from the requirement for flagella, other aspects of the behavior are poorly understood. Because the genetic basis of swarming is not well characterized, this behavior is well suited for comprehensive analysis using our approach.

In order to explore the genetic basis of swarming, we expressed this phenotype in terms of a quantitative selection, much as was done for swimming motility. A single round of enrichment consisted of inoculating our library of *E. coli* mutants onto the center of agar plates, incubating the plates to allow the cells to migrate outward from the site of inoculation, and transferring bacteria from the original area of inoculation to a fresh plate. After twenty rounds of daily successive transfers (Figure 3A), more than 90% of the population exhibited a defect in swarming (Figure S5). The enriched mutants were then subjected to microarray-based genetic footprinting.

As expected, the selection results were dominated by flagellar and chemotaxis genes (Figure 3B). While mutants with a defect in the flagellar apparatus did not swarm, chemotaxis mutants formed swarming patterns as finger-like projections, in contrast to the more uniform swarming patterns generated by the wild-type parent strain (Figure 3C). These observations indicate that the chemotaxis sensory system and flagellar switching have an effect on, but are not critical for, surface motility. Although this observation contradicts earlier studies on swarming in *E. coli* and *S. enterica* [29], more recent work has shown that chemotaxis mutants are capable of surface motility when the surface of the agar is sprayed with a fine mist of water [30], or when the agar concentration of the swarming media is reduced from 0.6% to 0.45% [31]. The microarray results (Datasets S7–S10) guided the interrogation of additional genes that may have a role in swarming. In addition to flagellar genes, we found other loci that also contribute to swarming motility (Table S1), which are discussed in more detail below.

Novel Genes Implicated in Swimming, Swarming, and χ-Phage Infection

Application of microarray-based genetic footprinting to swimming, swarming, and χ-phage selection was effective in identifying nearly all known flagellar and chemotaxis genes. Remarkably, the selection results guided the identification of three dozen additional genes that affect motility, most of which have no previous evidence of involvement in motility (Table S1). Most of these non-flagellar genes encode components of the cell envelope. For example, of the 20 non-flagellar genes revealed to affect swimming motility, twelve encode constituents of the inner membrane and periplasmic space. These gene products include transport proteins (SdaC, TatA, TatB, TatC, and WzxE), enzymes (DsbA and Prc), periplasmic glucan synthesis proteins (MdoG and MdoH), members of a signaling pathway (RcsC and RcsD), and a predicted inner membrane protein of unknown function (YrfF). Of these, only the genes encoding RcsD and glucan synthesis proteins had been previously implicated in swimming motility [32,33]. In addition, we identified several genes that encode cytoplasmic components and other genes of unknown function, including *fimE, hycG, intG, rep, ulaE,* and *yhjH*.

We systematically tested all newly identified swimming mutants for surface motility, and found that deletions of *dsbA, intG, prc, rcsC, rep, tatB, tatC, wzxE,* and *yrfF* strongly impair swarming. Surprisingly, while mutants with deletions of *rcsD, sdaC, tatA,* and *yhjH* were impaired in swimming, these mutants swarmed normally (unpublished data). Interrogation of genes with high *z*-scores in the enrichment for mutants incapable of swarming identified two additional genes that impact surface motility: *hns,* encoding a global transcriptional regulator, and *yfiR,* encoding a predicted periplasmic protein of unknown function. In-frame deletions of these genes abolished swarming; however, while the Δ*hns* mutant showed a severe swimming defect, the swimming motility of the Δ*yfiR* mutant was only mildly impaired (Figures 3D and 4). Among the loci exhibiting high *z*-scores after χ-phage selection were the *rfa* and *mdo* gene clusters responsible for the structural assembly of lipopolysaccharides (LPS) and osmoregulated periplasmic glucans (OPG). Genes involved with the synthesis of LPS and OPG precursors *(hldD, hldE, galU, gmhA, gmhB,* and *pgm)* were also highly abundant after χ-phage selection. These findings suggested that mutations in LPS and OPG biosynthetic genes may compromise motility. We confirmed this expectation by creating in-frame deletions of nearly all genes involved in LPS and OPG biosynthesis and assaying the mutants for motility. OPG mutants were defective in both swimming and swarming; surprisingly, however, only mutants with large LPS truncations showed significant defects in these behaviors (Figures 3E and 4).

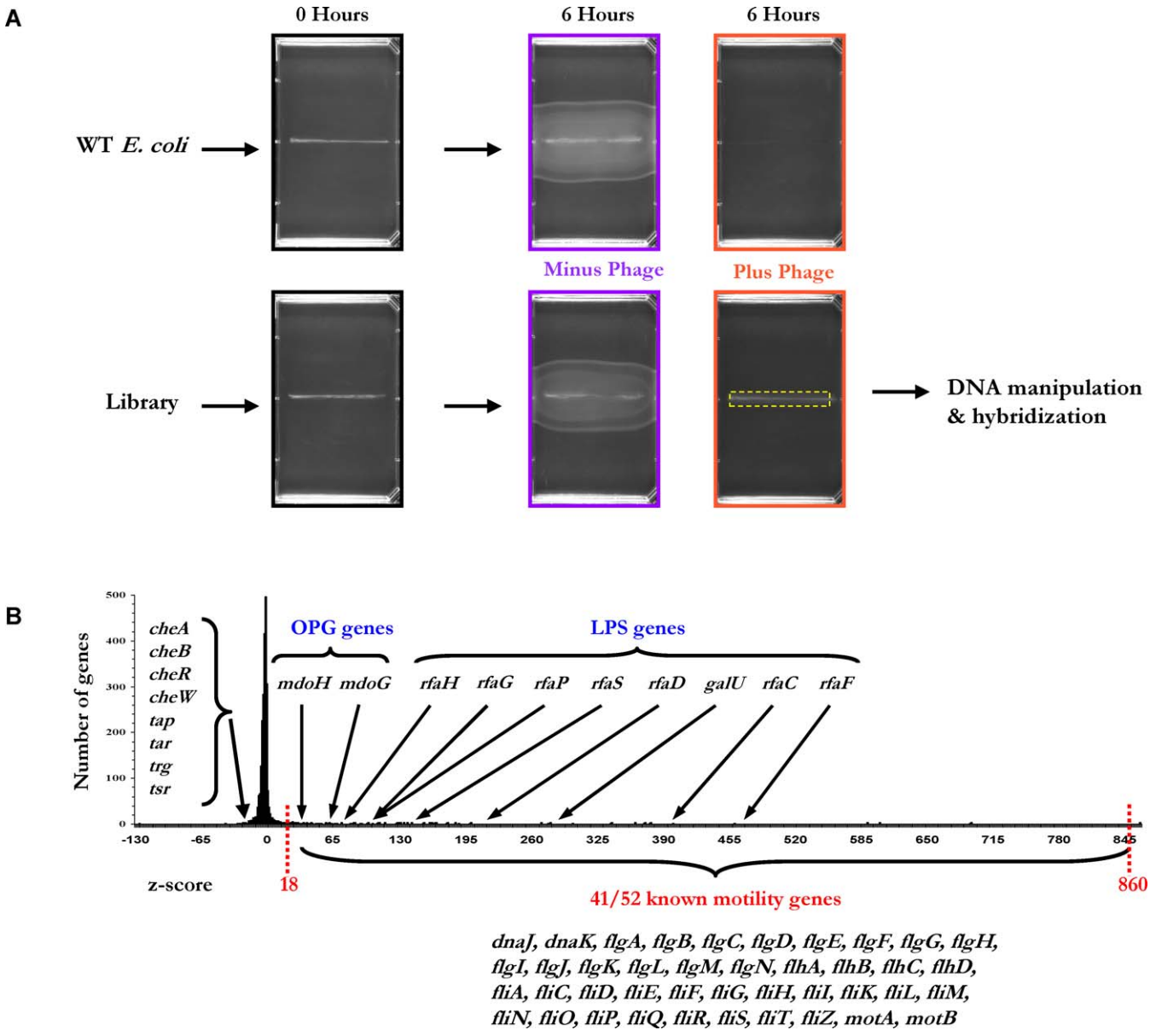

Figure 2. Selection against Bacteriophage χ Infection

(A) Soft-agar plates were inoculated with ~10^8 wild-type cells (top, black brackets) and an equal number of insertional mutants of the library (bottom, black brackets). In the absence of phage, wild-type (top, violet brackets) and mutant cells (bottom, violet brackets) can be seen migrating from the site of inoculation after 6 h of incubation. When phage is added to the soft-agar, wild-type cells are visually undetectable (top, orange brackets), whereas growth of mutants can be seen along the site of inoculation (bottom, orange brackets). The yellow dashed line indicates the area of the agar from which mutants were extracted for further analysis.

(B) Distribution of *z*-scores after selection against bacteriophage χ infection.

doi:10.1371/journal.pgen.0030154.g002

The wide functional repertoire of gene products found to affect motility prompted us to examine whether genetic perturbations in these loci affect motility by signaling upstream of the regulatory circuit that controls flagellar biogenesis, resulting in repression of the *flhDC* flagellar master operon. To investigate this possibility, we introduced *flhDC-lacZ* translational fusions in the deletion strains and performed β-galactosidase assays. Surprisingly, a large fraction of the mutants tested showed significant reduction in *flhDC-lacZ* expression values relative to the wild-type strain, demonstrating that the motility defects can be partly attributed to reduced expression of the *flhDC* operon. In addition, we noticed that LPS mutants varied widely in *flhDC* expression and that the repression of this operon, and the corresponding motility defect, were related to the degree of LPS truncation (Figure 4).

LPS and OPG Mutations Impair Motility by Repressing Flagellar Gene Expression through the Rcs Signaling Pathway

The widespread influence of LPS and OPG mutations on swimming, swarming, and χ-phage infection prompted us to explore the genetic mechanism of these mutations in more

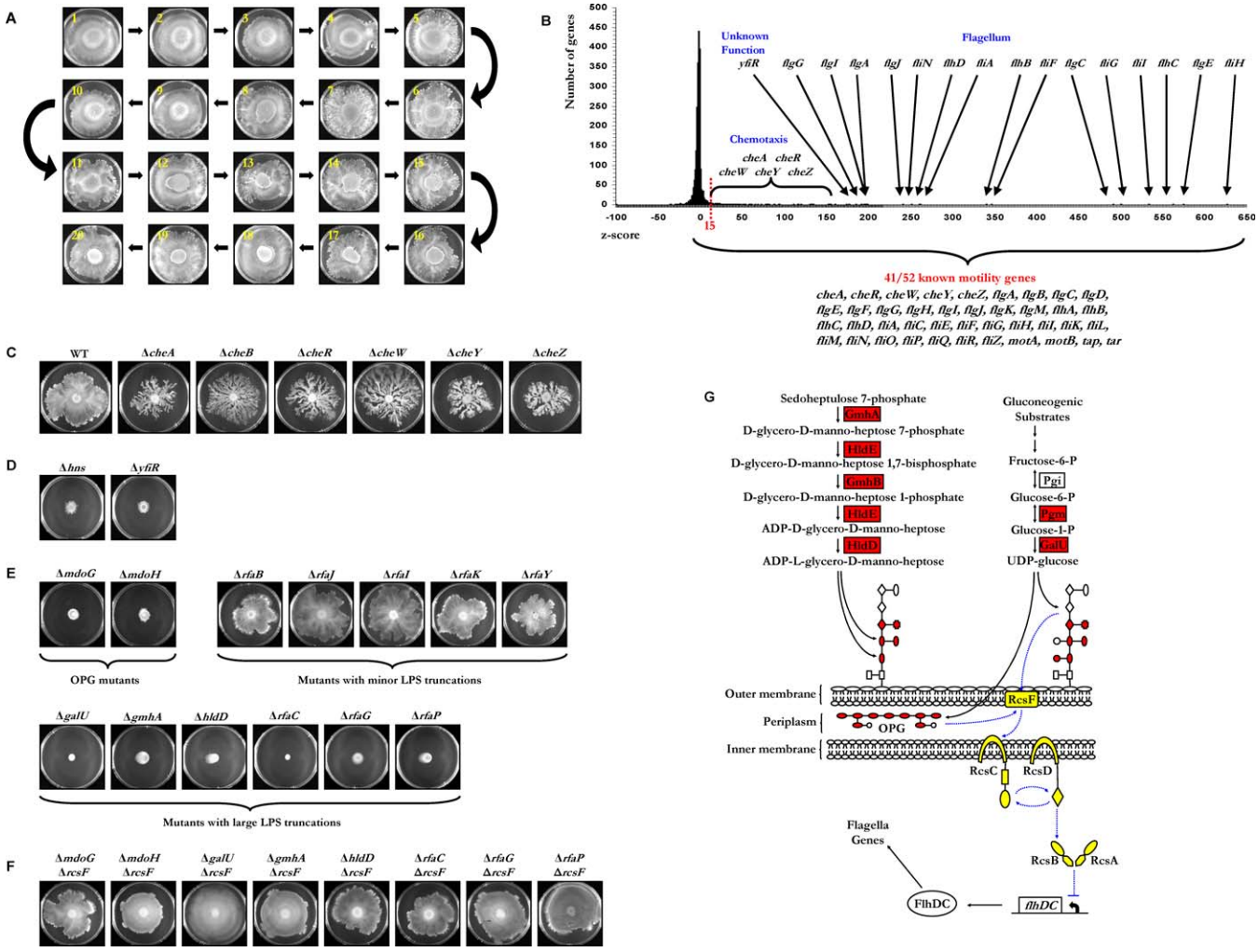

Figure 3. Systematic Identification and Analysis of Nonswarming Mutants

(A) Nonswarming mutants were enriched through twenty rounds of daily successive transfers. Plates imaged after each stage of enrichment show the gradual accumulation of nonswarming mutants at the center of the plates.
(B) Distribution of *z*-scores after enrichment for nonswarming mutants. Not shown is *flgD*, which has a *z*-score of 1,350.
(C) Images of the wild-type parent strain and chemotaxis mutants on swarm plates.
(D) Swarming motility of Δ*hns* and Δ*yfiR* mutants.
(E) Images of swarm plates with LPS and OPG mutants.
(F) Images of otherwise nonswarming LPS and OPG mutants with a Δ*rcsF* mutation.
(G) A model summarizing the involvement of Rcs signaling with swimming, swarming, and χ-phage infection. Components of the Rcs signaling pathway are shown in yellow. Mutations in the cellular components highlighted in red were found to impair swimming, swarming, and χ-phage infection by signaling through the Rcs phosphorelay pathway and repressing the expression of the *flhDC* operon. Black solid arrows denote precursor synthesis or gene expression. Blue dotted arrows denote signaling through the Rcs pathway.
doi:10.1371/journal.pgen.0030154.g003

detail. Previous evidence links LPS and OPG mutations to the activation of the Rcs phosphorelay system [34,35], and the Rcs system is known to negatively regulate the *flhDC* operon [36]. The Rcs pathway consists of a phosphotransfer protein (RcsD) that mediates phosphate transfer from a sensor kinase (RcsC) to a response regulator (RcsB) that binds DNA with an accessory protein (RcsA). Phosphorylated RcsB is known to bind upstream of the *flhDC* operon and to repress its expression. The pathway also includes a recently identified outer membrane lipoprotein (RcsF) that is known to activate the Rcs system [37]. To determine the role of the Rcs signaling pathway in LPS/OPG mediated repression of motility, we disrupted each of the components of the Rcs system in most of our LPS and OPG mutants. We found that deletion of *rcsB*, *rcsD*, or *rcsF* was sufficient to rescue motility in both LPS and OPG mutants (Figure S6), providing strong evidence that perturbations in these structures repress motility by signaling through the Rcs pathway. Deletion of *rcsC* rescued motility to a lesser extent. This observation is consistent with the dual functional role of RcsC as both kinase and phosphatase, moving phosphates both to and away from RcsB via RcsD, and that RcsB remains phosphorylated in *rcsC* null mutants [38,39]. Therefore, while *rcsC* mutations disrupt the RcsF→RcsC→RcsD→RcsB phosphorelay cascade, the phosphorylation of RcsB cannot be fully reversed in the absence of RcsC phosphatase activity, as observed by the reduced *flhDC-lacZ* expression and motility exhibited by *rcsC* and *rcsD* mutants (Figure 4). This conclusion is further supported by

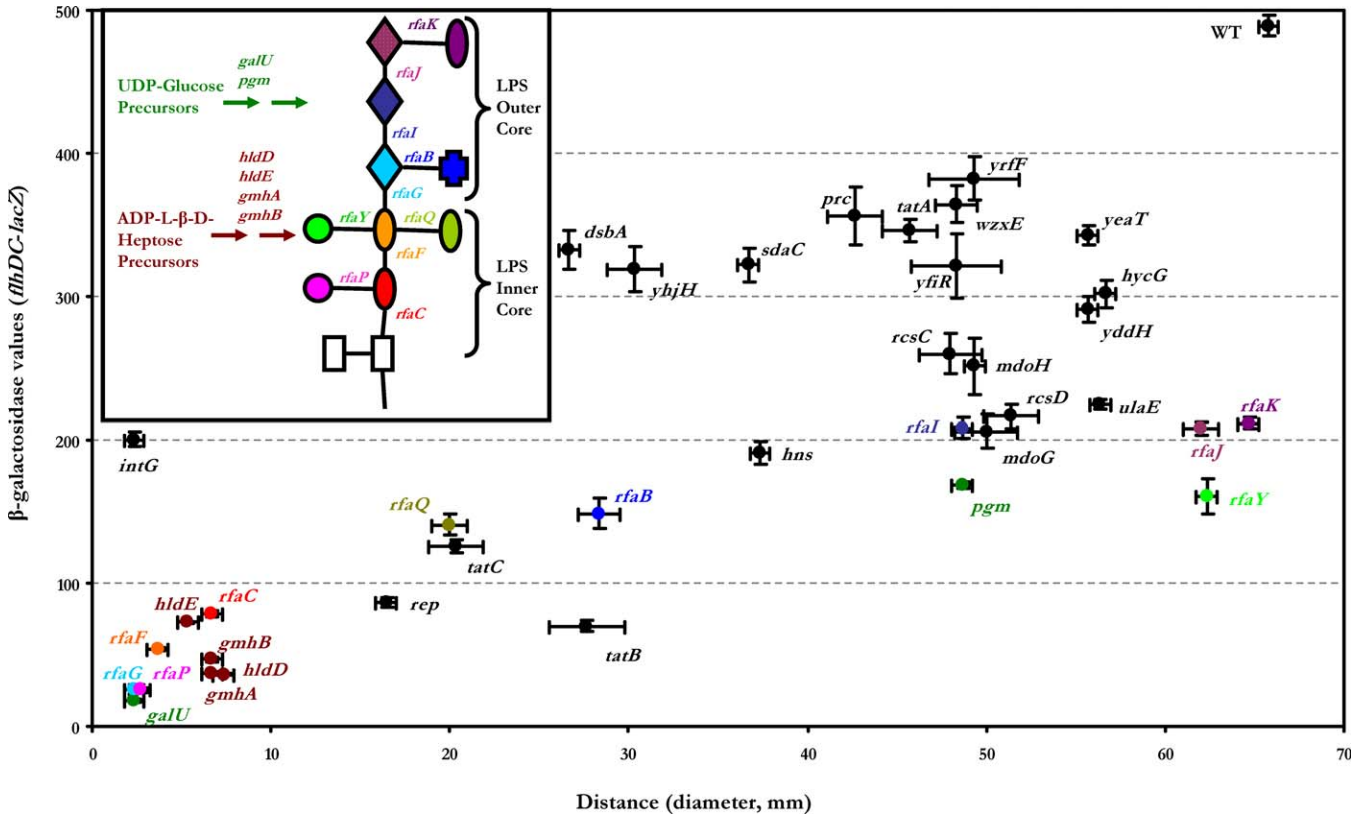

Figure 4. Motility and *flhDC-lacZ* Expression of Mutants

Motility was assayed by inoculating soft-agar with individual mutants and measuring the diameter of growth rings after incubation; error bars represent standard deviations of triplicate measurements. β-galactosidase assays were performed as described previously [77]; error bars represent standard deviations of three measurements. LPS structure is shown in the inset and genes responsible for the addition of each subunit of the LPS core are color coded; all other genes are in black. The wild-type parent strain appears in the top right-hand corner of the figure.

doi:10.1371/journal.pgen.0030154.g004

the dramatic reduction in swimming motility by *rcsC137* mutants (Figure S7), in which the *rcsC137* gene product has lost its phosphatase activity [40].

The χ-phage selection results suggest that LPS and OPG are necessary for infection. However, since functional flagella are a prerequisite for χ-phage infection, we sought to determine whether defects in LPS and OPG affect χ-phage infection directly or whether the observed selection results are primarily due to reduced flagellar expression. To evaluate the necessity of LPS and OPG for phage infection, we needed mutants that were defective in these structures but still synthesized functional flagella and were motile. Therefore, we created double mutants combining an LPS or OPG mutation and a secondary mutation in one of the components of the Rcs signaling pathway. These mutants were used in an infectivity assay in which plaque-forming units (PFUs) are monitored over time to assess sensitivity to phage infection [25]. An *flhD* mutant was used as a χ-phage-resistant control and, as expected, showed no sensitivity, whereas χ-phage multiplied rapidly in the presence of the wild-type strain (Figure 5A). Both OPG and LPS mutants showed decreased sensitivity to χ-phage, and the decrease in sensitivity was eliminated by introducing Δ*rcsF* deletions, indicating that OPG and LPS are not directly required for χ-phage infection (Figures 5B-D). We also observed that sensitivity to χ-phage was higher in *rfaI* mutants than *rfaC* mutants, indicating that χ-phage infectivity is directly related to the degree of *flhDC* expression (Figures 4, 5B, and 5C).

In a previous study, the swarming deficiency of LPS mutants had suggested an essential role for LPS in swarming behavior [41]. To test whether such a direct role exists, we interrogated our collection of LPS and OPG mutants for swarming proficiency. We found that mutants with OPG defects and severe LPS truncations were incapable of swarming and that introducing Δ*rcsF* deletions into these mutants was sufficient to rescue the phenotype (Figures 3F and S6). These data indicate that LPS and OPG are not directly necessary for swarming, and that the behavior exhibited by such mutants results from Rcs-mediated repression of the *flhDC* operon. A model summarizing the involvement of Rcs signaling on swimming, swarming, and χ-phage infection is shown in Figure 3G.

yhjH Affects Flagellar Motor Bias

Mutations in *yhjH* were recently found to impair swimming motility [42]. Consistent with this, we found that insertions in *yhjH* exhibit a high average *z*-score of +277 in our enrichment for nonmotile mutants. Surprisingly, this gene showed a negative *z*-score of −8 after bacteriophage χ selection, indicating that this mutant is impaired in swimming motility but may show increased susceptibility to χ-phage infection relative to the wild-type strain. Based on these observations, we hypothesized that this mutant has flagella with an extreme

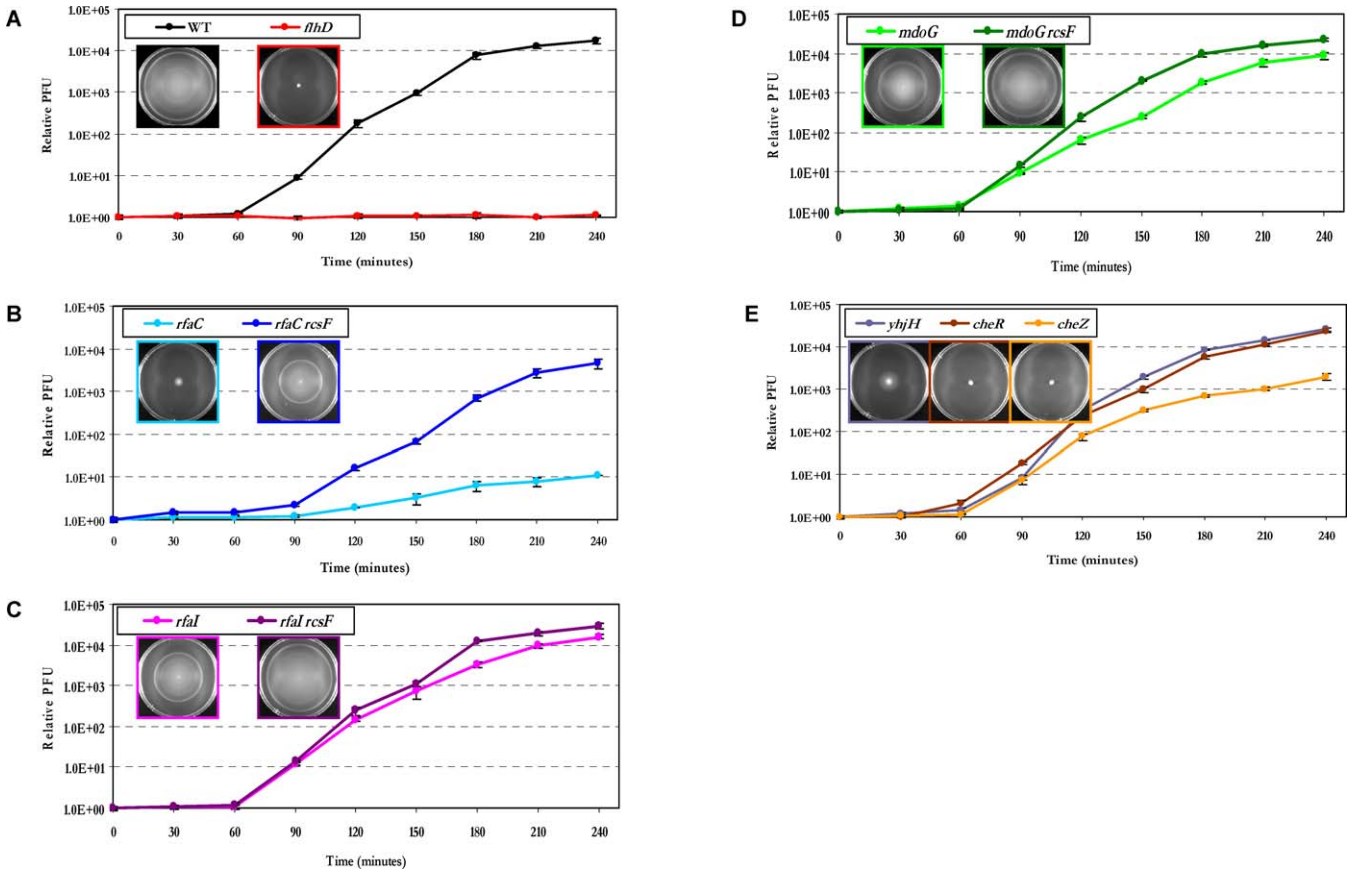

Figure 5. Quantitative χ-Phage Infectivity Assay

Log-phase cultures were inoculated with χ-phage at $t = 0$ min. Relative PFU was determined by the ratio of PFU at indicated time points to PFU at $t = 0$ min. Error-bars are standard deviations calculated from triplicate PFU counts. Plots were arranged to contrast the degree of infectivity between: (A) Wild type and *flhD*::kan; (B) Δ*rfaC* and Δ*rfaC*Δ*rcsF;* (C) Δ*rfaI* and Δ*rfaI*Δ*rcsF;* (D) *mdoG*::Tn and *mdoG*::Tn Δ*rcsF;* and (E) Δ*yhjH*, Δ*cheR*, and Δ*cheZ*.

doi:10.1371/journal.pgen.0030154.g005

CCW rotation bias, a phenotype also exhibited, to varying degrees, by *cheA*, *cheR*, and *cheW* mutants [43]. To further characterize the effect of this mutation on motility, an in-frame deletion of *yhjH* was constructed. Electron microscopy of Δ*yhjH* mutants showed the appearance of flagella, and light microscopy showed vigorous cellular movement (unpublished data), indicating that the flagella are capable of rotating; still, this mutant exhibited severe impairment in swimming (Figure 1C).

To determine whether the absence of *yhjH* alters the direction of flagellar rotation, several functional studies were performed. First, χ-phage infectivity assays with Δ*yhjH* mutants showed comparable levels of infection to *cheR* mutants (which exhibit CCW flagellar rotation bias) in contrast to the reduced sensitivity displayed by *cheZ* mutants (which have CW flagellar rotation bias), consistent with the *z*-scores of our χ-phage selection (Figure 5E). Second, while Δ*yhjH* mutants are impaired in swimming motility, they did not show a measurable defect in swarming (Figure 6A), which is in agreement with our finding that flagellar motor switching is not critical for swarming. In a final functional test, individual cells of four different strains—wild-type cells and mutants with *yhjH, cheR*, and *cheZ* deletions—were tethered to a microscope slide and the frequency of flagellar rotation switching was measured using computer tracking software in a fashion similar to Block et al. [44]. These measurements revealed that indeed the flagella of Δ*yhjH* mutants, while not strictly locked in one direction of rotation, exhibit a strong CCW bias with a rotational switching frequency intermediate between that found in wild-type cells and in Δ*cheR* mutants (Figure 6B). This finding is consistent with the χ-phage selection results. Tether assays with Δ*yhjH* Δ*cheZ* double mutants showed flagellar rotation indistinguishable from *cheZ* single mutants (unpublished data), indicating that null mutations in *cheZ* are epistatic to null mutations in *yhjH*. Together, these results indicate that the *yhjH* gene product is involved with the frequency of flagellar motor switching, a process that is among the remaining puzzles in bacterial chemotaxis [45].

Genome-Wide Identification of Genetic Interactions

The identification of novel genes that influence the expression of a phenotype is only the first step towards understanding its genetic basis. Gene products function within the context of highly interconnected structural and regulatory networks. We can dissect the genetic network context in which newly identified genes function by making libraries of double mutants in which a transposon library is constructed in the background of a mutation of interest. The phenotypic characterization of this library by a screen or selection can identify genetic interactions between the query mutation and all possible insertional mutations in the

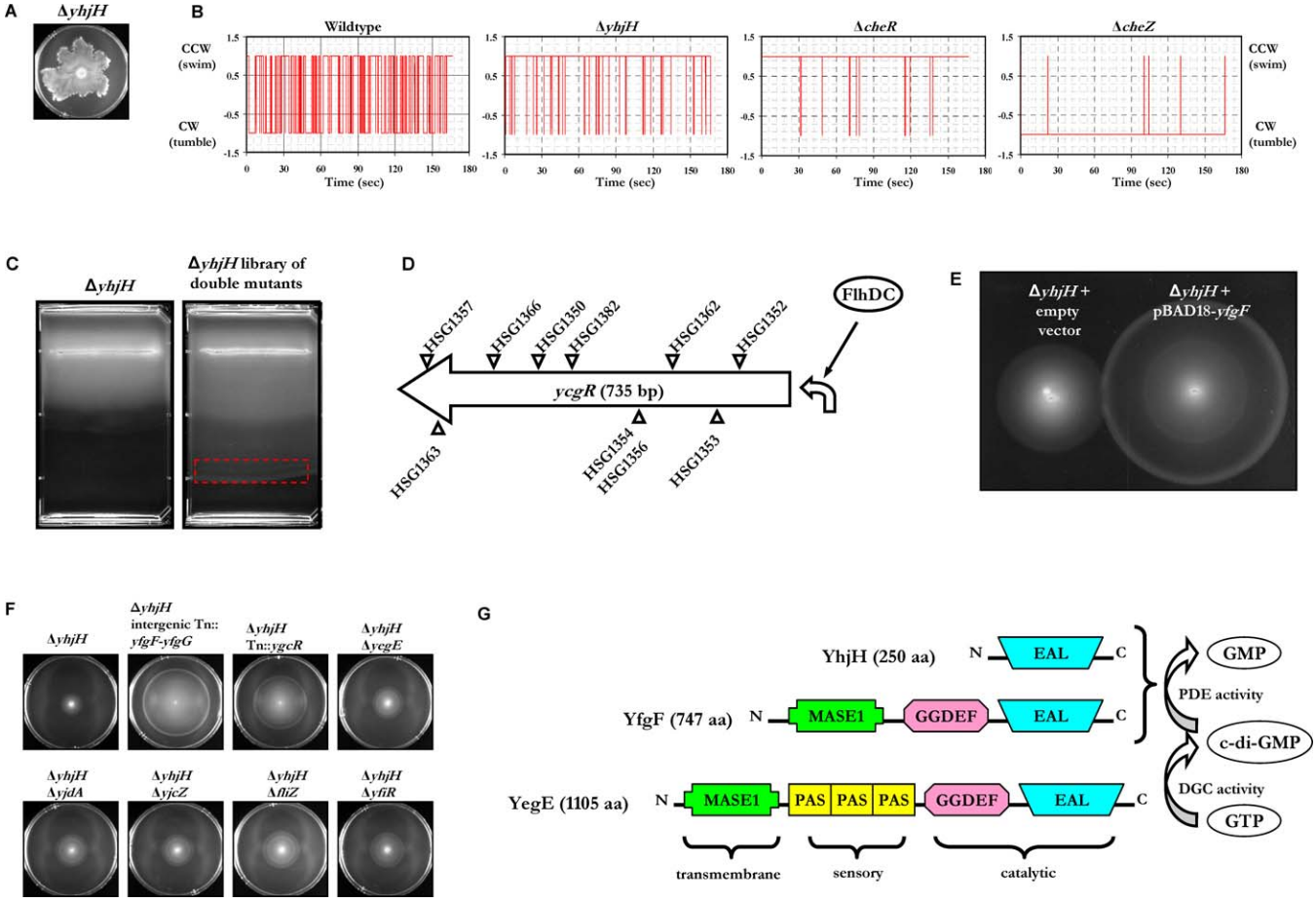

Figure 6. Identification and Analysis of Suppressors of the Δ*yhjH* Motility Defect

(A) Swarming behavior of the Δ*yhjH* mutant.

(B) Software-assisted tracking of tethered cells. The rotational direction of single motors were followed in time. CCW direction (swimming) is designated by 1 and CW direction (tumbling) is indicated by a −1. Wild-type cells switched frequently between the swimming and tumbling motor states while Δ*cheR* and Δ*yhjH* remained mostly in the swimming state. Averages and standard error are as follows: wild type, 0.32 ± 0.18, $n = 28$; Δ*yhjH,* 0.88 ± 0.10, $n = 22$; Δ*cheR,* 0.99 ± 0.03, $n = 23$; Δ*cheZ,* −0.99 ± 0.01, $n = 23$.

(C) Soft agar was inoculated with Δ*yhjH* mutants (left) and with a library of transposon insertional double mutants (right). After a 20-h incubation at 30 °C, mutants that showed a suppression of the motility defect were extracted from the agar (red dashed line) and used for further analyses.

(D) The *ycgR* transcriptional unit is shown. Ten insertional mutations were mapped to nine different locations in the *ycgR* gene. Triangles denote the sites of the insertions; strain names appear next to each insertion site. Triangles above the gene indicate transposon insertions with the T7 promoter oriented to the right, and triangles below represent the promoter facing the left. Transcription of *ycgR* is positively regulated by FlhDC [83].

(E) Expression of *yfgF* partly suppresses the motility defect of the Δ*yhjH* mutant. Wild-type and mutant strains were transformed with empty pBAD18 or with pBAD18 carrying *yfgF* cloned in front of the arabinose-inducible promoter. Overnight cultures were used to inoculate soft agar plates containing 100 μg/ml ampicillin and 0.2% arabinose. Images were taken after 8 h at 30 °C.

(F) Double mutants were generated (as described in Protocol S2) based on microarray results. Displayed are mutants that show partial suppression of the Δ*yhjH* motility defect.

(G) Domain organization of YhjH, YfgF, and YegE with predicted biochemical activities in *E. coli*. Domain structure is diagrammed according to Pfam (http://www.sanger.ac.uk/Software/Pfam). PDE, phosphodiesterase; DGC, diguanylate cyclase; PAS, ubiquitous signal sensor domain [86]; MASE1, membrane-associated sensor domain [87]; GMP, guanosine monophosphate; and GTP, guanosine triphosphate.

doi:10.1371/journal.pgen.0030154.g006

genome, thereby revealing the local genetic context in which the query locus functions to influence the phenotype. Systematic analyses of such interactions in yeast [46,47] are providing a wealth of knowledge about gene function and pathway organization. An important class of such interactions is suppressor mutations that either partially or fully restore the phenotype deficits of a query mutation. In a genome-wide effort to identify suppressors of swimming defects, additional libraries of transposon insertional mutants were created in genetic backgrounds containing gene deletions of interest.

Secondary insertional mutations were observed to suppress motility defects in Δ*hns* and Δ*yhjH* genetic backgrounds (Figures 6C and S8A). These suppressor mutations were identified by inoculating soft-agar plates with $\sim 10^8$ double mutants and extracting cells from the motile front after ~20 h of incubation at 30 °C. A sample of suppressor mutants extracted from the extreme edge of the motile front was used for both microarray-based genetic footprinting, and for isolation of individual mutants for subsequent characterization. Transposon insertion sites were identified in individual clones by applying the genetic footprinting procedure outlined in Figure S1.

Among the 18 suppressor mutants sampled at random

from the Δ*yhjH* background, half had insertions in different regions of *ycgR*, a gene encoding a protein of unknown function (Figure 6D). This finding is consistent with a recent report in which the inactivation of *ycgR* was observed to improve motility of *yhjH* mutants [48]. The other half of Δ*yhjH* suppressor mutations were found to contain insertions within the intergenic region between the divergently transcribed genes *yfgF* and *yfgG*, which encode gene products of unknown function. P1 transduction of this insertion to the Δ*yhjH* isogenic background confirmed the ability of the insertion to suppress the motility defect (unpublished data). However, deletions of either *yfgF* or *yfgG* produced no measurable difference in motility in the Δ*yhjH* background (Figure S9). Conversely, overexpression of *yfgF* (but not *yfgG*) was found to suppress the motility defect of Δ*yhjH* mutants (Figure 6E). Microarray-based genetic footprinting of the entire pool of mutants extracted from the motile front guided the identification of five additional suppressor mutations (Figure 6F; Dataset S11). Among the loci that partially suppress the motility defect of *ΔyhjH* are *fliZ* (a gene predicted to be a regulator of the flagellum-specific sigma factor sigma28), *yfiR* (a gene identified in the selection for swarming motility defective mutants), and three additional genes of unknown function: *yjdA*, *yjcZ*, and *yegE*.

We hypothesize that mutations partially suppressing the chemotaxis defect of Δ*yhjH* mutants do so by correcting the severe CCW flagellar rotation bias. When combined in the same background, these mutations may bring the motor bias closer to the optimal operating point for chemotaxis, either by having an opposing effect on the intracellular concentration of signaling molecules known to affect motility (discussed in the next section) or by an unknown mechanism that overrides the CCW bias. Further studies are underway to explore the functional relationship between *yhjH* and these suppressor mutations. The mechanisms by which deletion of *yegE* and overexpression of *yfgF* suppress the motility defect of Δ*yhjH* mutants are discussed in the next section. Suppressor mutations identified in the Δ*hns* background are shown and discussed in Figure S8, and the microarray results can be found in Dataset S12.

The Role of the C-di-GMP Second-Messenger System in Swimming and Swarming Motility

Based on sequence homology, YhjH, YfgF, and YegE belong to the newly identified and highly prevalent family of proteins that function in the turnover of bis-(3′-5′)-cyclic dimeric guanosine monophosphate (c-di-GMP), which is a second messenger involved in the regulation of a wide variety of bacterial behaviors [49]. Synthesis of c-di-GMP is catalyzed by diguanylate cyclases (DGC) and its degradation is regulated by phosphodiesterases (PDE). The cyclase and phosphodiesterase activities have been attributed to GGDEF and EAL protein domains, respectively [50,51], and the activity of these domains is known to have opposite effects on motility [52]. YhjH contains an EAL domain, and expression of this protein leads to the degradation of c-di-GMP and enhanced motility in *S. enterica* [52]. Based on this observation and because EAL domain proteins function in the degradation of c-di-GMP, we hypothesized that the motility defect of Δ*yhjH* (Figure 1C) is a result of increased intracellular levels of c-di-GMP.

YegE and YfgF both contain an EAL domain C-terminal to a GGDEF domain (Figure 6G). The presence of domains of opposing activities in a single protein complicates functional inferences. However, a single GGDEF/EAL composite protein exhibiting concomitant DGC and PDE activities has not been reported. In addition, several GGDEF/EAL composite proteins were found to exhibit either DGC or PDE activity [53,54]. Based on the known antagonistic effects of c-di-GMP on motility [52] and by following several lines of reasoning, we hypothesized the dominant enzymatic activities of the GGDEF and EAL domains in YfgF and YegE. We argue that YfgF has an active EAL domain and functions as a PDE based on three observations: (1) expression of this gene enhances motility of the Δ*yhjH* strain (Figure 6E); (2) the amino acid sequence of YfgF shows similarity to enzymatically active EAL domains (Figure S10); and (3) the amino acid sequence lacks a complete GGDEF motif needed for DGC activity (data not shown). Likewise, three observations suggest that the EAL domain in YegE is inactive and that this protein functions primarily as a DGC: (1) deletion of YegE enhances motility of the Δ*yhjH* strain (Figure 6F); (2) the amino acid sequence of the EAL domain in YegE is not consistent with an enzymatically active form (Figure S10); and (3) YegE contains an intact GGDEF motif (data not shown). Based on these observations, we propose that deleting *yegE* and over-expressing *yfgF* suppress the motility defect of the Δ*yhjH* strain by reducing the intracellular levels of c-di-GMP (Figure 7). Deletion of *yegE* and over-expression of *yfgF* did not have significant effects on the motility of the wild-type strain (unpublished data).

E. coli has 19 genes encoding proteins with GGDEF domains [55]. If c-di-GMP levels act globally and can influence motility, then insertions in many of the genes containing active GGDEF domains should rescue motility in the Δ*yhjH* double mutant library. However, the results of the genome-wide screen for suppressors of the Δ*yhjH* motility defect reveals that this is not the case (Table S2). These observations suggest that the expression and/or enzymatic activities of these GGDEF-containing proteins may be under precise context-dependent control. Alternatively, specificity in c-di-GMP signaling may be due to a number of mechanisms including spatial and temporal sequestration, microcompartmentalization, restricted production/degradation, or target modification [56].

The manner in which c-di-GMP alters motility at the molecular level is currently unknown. However, it has been reported that c-di-GMP binds to the PilZ domain of the aforementioned YcgR protein [48]. It is hypothesized that YcgR undergoes a conformational change upon binding to c-di-GMP, and that the YcgR-c-di-GMP complex impairs motility through a protein–protein interaction with the flagellar motor [57]. Such an interaction may explain the observed rotational bias of flagella in Δ*yhjH* mutants (Figure 6B) and is in agreement with our finding that mutations in *ycgR* strongly suppress the motility defects of Δ*yhjH* mutants (Figure 6F).

In addition to its effects on swimming, we found evidence that c-di-GMP signaling also plays a role in swarming motility. As stated previously, mutations in *yfiR* strongly abolish swarming motility. The *yfiR* gene is the first in an operon that also contains *yfiN* and *yfiB* (inset of Figure 7). The arrangement of these genes in an operon suggests that they may function together. YfiR is predicted to be a periplasmic protein, YfiB shows sequence similarity to outer-membrane

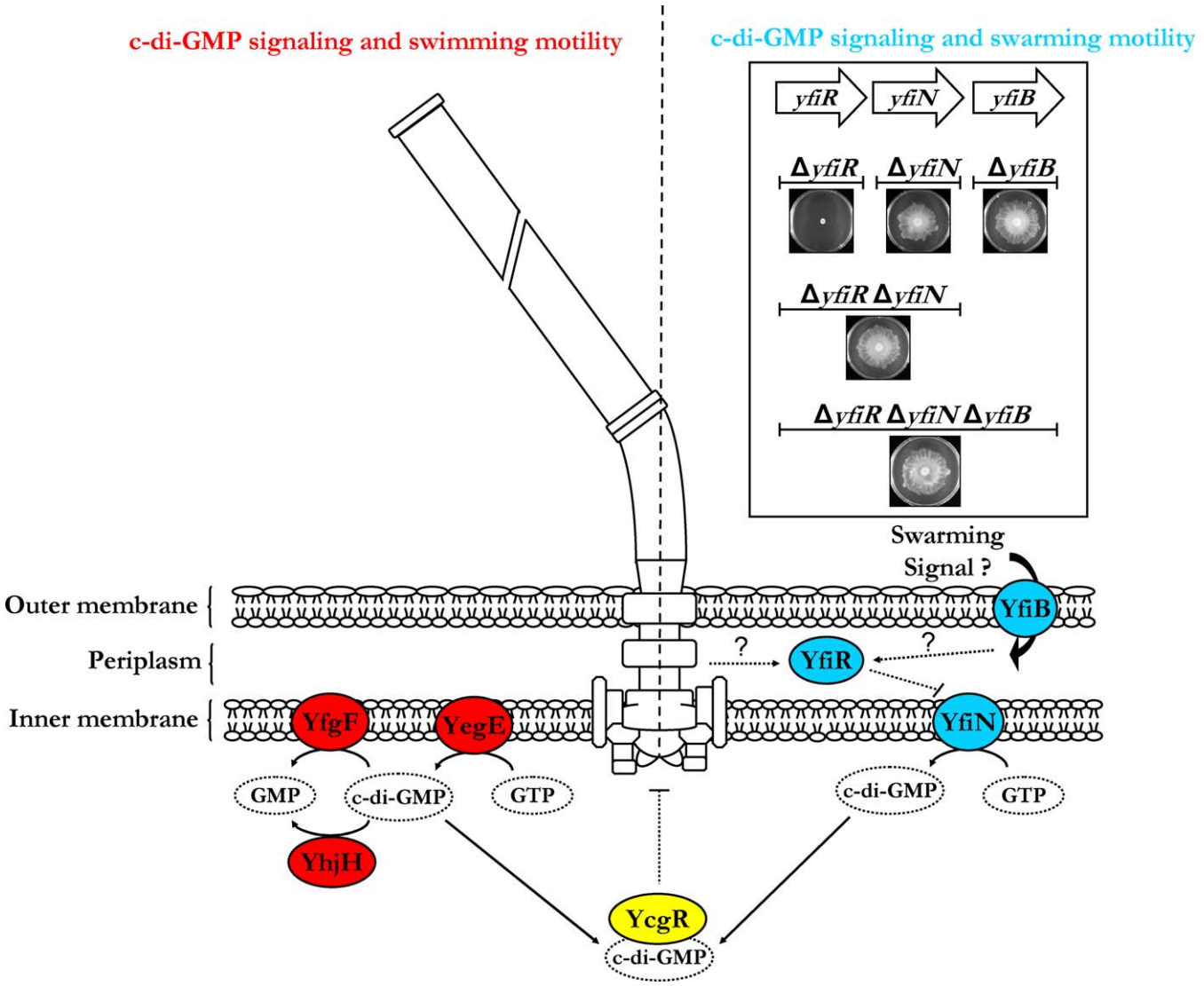

Figure 7. A Model Illustrating the Influence of C-di-GMP Signaling on Swimming and Swarming Motility

Genetic evidence suggests that the c-di-GMP second-messenger system is involved in swimming and swarming motility. The gene products are color coded according to the following scheme: red for swimming and blue for swarming. The interaction of the YcgR-c-di-GMP complex (highlighted in yellow) with the flagellar motor is represented by a black dotted line. Question marks represent unknown signals for swarming: for example, YfiR may be activated by flagella unable to rotate on solid agar or by an extracellular agent that passes through YfiB, which is predicted to be a porin protein. The inset shows the effects of gene deletions on swarming.

doi:10.1371/journal.pgen.0030154.g007

porin proteins, and YfiN is a predicted inner-membrane protein with GGDEF and HAMP domains. We found that deletion of *yfiN* strongly suppresses the swarming defect of the Δ*yfiR* strain, indicating that *yfiR* is genetically upstream of *yfiN*, and that YfiR may regulate the DGC activity of YfiN's GGDEF output domain by interacting with the HAMP sensory input domain (Figure 7). Mutations in *ycgR* were also found to suppress the swarming defect of the Δ*yfiR* strain (unpublished data), suggesting that YcgR binds c-di-GMP to affect both swimming and swarming motility. The observations that the Δ*yhjH* mutant is impaired in swimming but indistinguishable from the wild-type strain in swarming, while in contrast the Δ*yfiR* strain cannot swarm and is only mildly impaired in swimming, support the notion that c-di-GMP signaling pathways are temporally and/or spatially separated, as recently suggested by others [58,59].

Involvement of Type 1 Fimbriae in Swimming Motility

The abundance of *fimE* and *fimB* mutants in the enrichment for nonmotile mutants suggested a role for type 1 fimbriae in swimming motility. These genes encode site-specific recombinases that catalyze the inversion of a DNA element known as the *fim* switch or *fimS*, whose orientation controls the expression of fimbrial structural genes [60]. Inversion of *fimS* by site-specific recombinases alternately connects and disconnects the fimbrial structural genes from their promoter, resulting in a process of phase variation that gives rise to bacteria in either the fimbriate (phase ON) or afimbriate (phase OFF) state [61]. By randomly sampling mutants impaired for motility and sequencing the region of DNA adjacent to the transposon, we identified a mutant with a reduced ability to swim with an insertion within *fimS*. To determine the nature of the motility defect, we analyzed the

fimS mutant by transmission electron microscopy. The *fimS* mutant exhibited a level of fimbriation similar to *fimB*$^-$ *fimE*$^-$ double mutants locked in phase ON (Figure S11A), indicating that a high level of fimbriation reduces motility in semi-solid agar. This observation is confirmed by comparing the motility of the *fimS* mutant to phase ON *fimB*$^-$ *fimE*$^-$ double mutants (Figure S11B). We found that swarming was not impaired in either the *fimS* mutant or the mutants with fimbria locked in phase ON, indicating that fimbria expression does not interfere with swarming motility (Figure S11C). The basis for motility suppression by constitutive fimbriae expression remains unclear; however, we observed that hyper-fimbriated cells tend to have, on average, fewer flagella compared to their afimbriated counterparts (Figure S11D). This may reflect competing demands for resources and/or surface area for synthesis and assembly of these extracellular appendages.

The Genetic Basis of Environmentally Induced Repression of Motility

Chemotaxis in *E. coli* is strongly inhibited by environmental conditions such as high temperature, low pH, and high osmolarity [62–64]. Some of these environmental influences may be due to direct physicochemical perturbations to chemotaxis or flagellar function. Alternatively, these signals may provide crucial information about the cell's local environment, influencing chemotactic behavior through upstream regulatory pathways. Consistent with this picture, the promoter of the *flhDC* operon, the master regulator of flagellar gene expression, is one of the most highly regulated loci in the genome and contains many transcription-factor binding sites [65]. We devised a simple selection strategy to identify the genetic loci that contribute to environmentally induced variation in chemotactic behavior. We focused on inhibition of motility by high osmolarity (0.5 M NaCl), since previous evidence suggested that this environmental condition signals to the *flhDC* regulatory region [66]. We reasoned that null mutations in components of such upstream signaling pathways would alleviate repression of chemotaxis under high [NaCl] conditions. According to this model, the transposon insertion library should harbor mutants that perform chemotaxis in high [NaCl] as well as wild-type cells do under low [NaCl] conditions. As can be seen in Figure S12A, this is in fact what we observe since, during the same time interval, some members from the transposon mutant library travel significantly further away from the site of inoculation than do the homogeneous population of wild-type cells. In order to identify the mutations associated with the observed alleviation in suppression of motility under high [NaCl], we extracted the population of mutants that traveled to the extreme edge of the chemotaxis front. Microarray-based genetic footprinting of these mutants provided quantitative genome-wide readout of the population (Dataset S13).

The selection results revealed that mutants harboring insertions in five genes (*ompR, envZ, znuA, znuC,* and *yfiM*) were the most abundant. The microarray results were confirmed by showing that individual strains with mutations in these genes showed increased motility in high [NaCl] relative to the wild-type strain (Figure S12B). OmpR and EnvZ are well-characterized members of the two-component osmoregulatory system (Figure S12C). EnvZ is the sensor kinase that phosphorylates OmpR, a DNA-binding regulatory protein, under conditions of high osmolarity [67]. Our finding that the EnvZ/OmpR signaling pathway mediates motility suppression in high [NaCl] is consistent with previous work that found phosphorylated OmpR to negatively regulate the expression of flagella by interacting with the promoter region of *flhDC* [66]. ZnuA and ZnuC are part of a high-affinity zinc uptake system. The role of *yfiM*, a novel uncharacterized gene that shows sequence similarity to a lipoprotein, is not clear at this point. Ongoing work will determine how the gene products of *yfiM, znuA,* and *znuC* contribute to this signaling pathway, either through Envz/OmpR or through a parallel pathway.

We have shown that the limits on swimming motility under nominally extreme conditions can be regulated by "interpretation" of environmental signals rather than by hard physicochemical constraints on energy generation or mechanics. This argues for a more nuanced perspective on the functional constraints influencing bacterial behavior in general—including the strong coupling between behavior and environment—and an appreciation of the rich ecological context that has shaped bacterial behavior on geological time scales.

Conclusions and Summary

Microbes account for half the world's biomass and are the most widely distributed organisms on the planet. Yet most of our genetic understanding of bacterial behavior comes from the tiny fraction of microbes studied in the laboratory. With the recent advances in bacterial whole-genome sequencing [68,69], the scientific community is poised to take systems-level experimental approaches to rapidly reveal novel and fundamental insights into the microbial world. In this study, we have established a powerful framework for the efficient and comprehensive identification of the genetic basis of complex bacterial behaviors. The power of this approach lies in the rapid and parallel manner in which positive and negative genetic contributions can be mapped to any phenotype after competitive selection. We demonstrated this approach in four distinct but complementary selections to reveal the genetic basis of *E. coli* motility. Using this framework, we identified greater than 95% of previously known flagellar and chemotaxis genes, and we found three dozen novel contributors to motility consisting of both characterized and uncharacterized genes. Although similar approaches have been successfully applied to the study of pathogenicity [70–74], the large number of genes reported and the limited analyses of individual mutants made it difficult to determine whether the methods employed in these studies could detect the subtle quantitative differences necessary to map genetic loci with high sensitivity and specificity. In this study, we confirmed our findings by functional analyses of individual mutants, which revealed high levels of sensitivity and low rates of false positives. In addition, we have shown that the same method can be used to quickly and thoroughly explore the genetic interactions between a single locus and all other genetic loci in the genome. These interactions correspond to important network-level concepts; for example, the flow of information within signal transduction pathways and second-messenger systems such as c-di-GMP. In addition to identifying gene-by-gene interactions, we have shown that the same framework can be used to reveal gene-by-environment interactions that

are crucial for understanding function within the rich ecological context in which genetic networks have evolved.

Materials and Methods

Strains and microbiological techniques. All strains used in this study are isogenic derivatives of *E. coli* MG1655 [75] and are listed in Table S3. Bacteriophage and plasmids used in this study are listed in Table S4, and oligonucleotide sequences can be found in Table S5. Transposon mutant libraries were constructed using hyperactive Tn5 EZ::TN transposase (1.0 U/μl; Epicentre Technologies, http://www.epibio.com/) according to the manufacturer's guidelines. Chromosomal markers were transferred by generalized transduction with P1*vir* [76]. β-galactosidase measurements were performed in triplicate using a microtiter assay as described previously [77]. Additional molecular techniques are described in Protocol S2.

Selection for nonmotile mutants. Motility soft agar plates were prepared using OmniTray Single Well plates (Fisher Scientific, https://www.fishersci.com/) containing tryptone broth (13 g Bacto tryptone and 7 g NaCl per liter) and 0.25% Difco agar. Plates prewarmed to 30 °C were inoculated with 10 μl of the transposon library containing 10^{10} cells/ml by stabbing the agar with a pipette tip and expelling the cells horizontally along the center of the short length of the plate. After 8 h at 30 °C, mutants remaining at the site of inoculation were transferred to a fresh plate by aseptically plunging a sterile coverslip (Corning, http://www.corning.com/) into the agar at the site of inoculation and inserting the coverslip into a fresh motility agar plate at an identical position. This step was repeated to enrich for nonmotile mutants. Cells were harvested from the site of inoculation after each stage of enrichment and frozen at −80 °C in 15% glycerol.

Selection and infectivity assay with bacteriophage χ. Bacteriophage χ (ATCC 9842B) was aseptically added to motility agar after autoclaving to a final concentration of 10^9 PFU/ml. Plates prewarmed to 30 °C were inoculated along the center with the transposon library that was grown to an OD_{600} of 0.6. After 6 h of incubation at 30 °C, mutants were harvested from the site of inoculation. Infectivity with bacteriophage χ was assayed as described previously with minor modifications [25]. Wild-type and mutant strains were cultured to mid-log phase at 30 °C with aeration in 10 ml of tryptone broth, at which point 100 μl of χ-phage was added to a final concentration of 10^6 PFU/ml, and the bacterial cell and χ-phage mixture was incubated at 30 °C with shaking. Every 30 min for 4 h, 100 μl of the bacteria/phage mixture was removed, diluted, and 100 μl of each diluted sample were added to 3 ml of top agar (TB, 0.5% agar), along with 100 μl of log-phase wild-type *E. coli*, and poured over hard-agar plates (TB, 1.0% agar). Plates were incubated at 30 °C for 24 h. Relative PFU is the ratio of PFUs at each time point to the PFU at 0 min.

Swarming motility assay. Media for swarming assays consisted of 10 g of Bacto peptone, 3 g of Difco beef extract, 5 g of NaCl, and 4.5 g of Eiken agar (Eiken Chemical, http://www.eiken.co.jp/) per liter. Glucose was added after autoclaving at 5 g/L. Swarm agar plates were allowed to dry overnight at room temperature and preheated to 30 °C before use. To enrich for mutants that fail to swarm, the surface at the center of a swarm plate was inoculated with $\sim 10^6$ cells of the transposon library at mid-log phase of growth. After 24 h at 30 °C, bacteria from a centimeter square area at the center of the agar was aseptically removed, placed into a test tube containing 5 ml of LB prewarmed to 30 °C, and incubated with shaking to an OD_{600} of 0.5. Ten microliters of this culture was used to inoculate a fresh swarm plate. This procedure was repeated a total of 20 times to enrich for nonswarming mutants. A small sample of cells harvested from the site of inoculation after each stage of enrichment was frozen at −80 °C in 15% glycerol.

Motility assays in high-salt conditions. Motility agar plates were prepared with 500 mM NaCl. The prewarmed agar was inoculated 2.5 cm from one side of the long end of the plates with a 10-μl aliquot of 10^8 transposon insertional mutants. The plates were incubated at 30 °C for 32 h. As a comparison, wild-type cells were treated similarly. The mutants that traveled furthest at the edge of the motile front were harvested for subsequent genetic footprinting.

Genetic footprinting and DNA manipulations. Samples of $\sim 10^7$ cells were suspended in a mixture of NEB Buffer 2 and 5% Triton X-100, lysed by incubating at 99 °C for 40 s, divided into two equal volumes, and treated separately with HinP1 and MspI, in conjunction with alkaline phosphatase. After the restriction enzymes were heat inactivated, the digestion products were combined, ethanol precipitated, and ligated to a partially double-stranded Y-shaped linker [78]. Ligation products were purified using QIAquick gel extraction columns (Qiagen, http://www1.qiagen.com/), treated with *E. coli* DNA polymerase I (New England Biolabs, http://www.neb.com/), and used as template in a PCR containing a primer specific to the transposon and a primer specific to the Y-shaped linker, 0.2 mM dNTP mix, PCR buffer, and ExTaq DNA polymerase (TaKaRa, http://www.takara-bio.com/). Cycling conditions were 94 °C for 2 min; 30 cycles of 94 °C for 30 s, 68 °C for 30 s, and 72 °C for 3 min; and 72 °C for 10 min. The following improvements were made to a previously described method [12]: (1) heat lysis with Triton X-100 eliminated the need to extract DNA from large quantities of cells; (2) digestion products were treated with alkaline phosphatase to remove the 5′ phosphate, thereby preventing the chromosomal DNA from self ligating; and (3) after ligation, the break in the DNA between the chromosomal DNA and the Y-linker was repaired by treating with *E. coli* DNA polymerase I in the presence of 0.1 mM dNTP mix. These improvements have significantly increased signal to noise and have also provided the means to work with a small quantity of cells.

Tethering assay. Cells were tethered as described previously [44] and were visualized using phase microscopy (Nikon 50i, 40× objective; Nikon, http://www.nikonusa.com/) and a CCD camera (Basler A601f; Basler, http://www.basler.com/). Images of cells were captured at 60 frames per second. The center of mass position of the cells was measured in real time using custom software written in LabVIEW (National Instruments, http://www.ni.com/). The flagellar motor bias was calculated using custom software written in MATLAB (Mathworks, http://www.mathworks.com/) or LabVIEW. The angular velocity was computed from the center of mass position time series data. The bias for a 166-s interval was calculated as the fraction of time individual cells were spinning in a positive direction. In our system, this corresponds to the CCW rotational bias.

Supporting Information

Dataset S1. Unselected Library Replicates

Found at doi:10.1371/journal.pgen.0030154.sd001 (629 KB XLS).

Dataset S2. Microarray Data for Swimming Motility Replicate 1

Found at doi:10.1371/journal.pgen.0030154.sd002 (557 KB XLS).

Dataset S3. Microarray Data for Swimming Motility Replicate 2

Found at doi:10.1371/journal.pgen.0030154.sd003 (544 KB XLS).

Dataset S4. Microarray Data for Swimming Motility Replicate 3

Found at doi:10.1371/journal.pgen.0030154.sd004 (552 KB XLS).

Dataset S5. Microarray Data for Bacteriophage χ Selection Replicate 1

Found at doi:10.1371/journal.pgen.0030154.sd005 (553 KB XLS).

Dataset S6. Microarray Data for Bacteriophage χ Selection Replicate 2

Found at doi:10.1371/journal.pgen.0030154.sd006 (544 KB XLS).

Dataset S7. Microarray Data for Swarming Motility Replicate 1

Found at doi:10.1371/journal.pgen.0030154.sd007 (557 KB XLS).

Dataset S8. Microarray Data for Swarming Motility Replicate 2

Found at doi:10.1371/journal.pgen.0030154.sd008 (549 KB XLS).

Dataset S9. Microarray Data for Swarming Motility Replicate 3

Found at doi:10.1371/journal.pgen.0030154.sd009 (549 KB XLS).

Dataset S10. Microarray Data for Swarming Motility Replicate 4

Found at doi:10.1371/journal.pgen.0030154.sd010 (549 KB XLS).

Dataset S11. Microarray Data for Motility Selection of the ΔyhjH Double Mutant Library

Found at doi:10.1371/journal.pgen.0030154.sd011 (548 KB XLS).

Dataset S12. Microarray Data for Motility Selection of the Δhns Double Mutant Library

Found at doi:10.1371/journal.pgen.0030154.sd012 (550 KB XLS).

Dataset S13. Microarray Data for Motility under High Salt Conditions

Found at doi:10.1371/journal.pgen.0030154.sd013 (553 KB XLS).

Figure S1. Parallel Amplification of Transposon-Adjacent Sequences

Genomic DNA extracted from a sample of transposon insertional mutants is restriction digested. Digested fragments are ligated to a partially double-stranded Y-shaped linker. In the initial PCR cycle,

primer annealing to a sequence within the transposon and DNA polymerase-mediated extension generates a double-stranded DNA template. In subsequent PCR cycles, primers annealing to a region within the transposon and the top strand complement of the Y-linker allows exponential amplification of the transposon-adjacent sequences. The presence of a T7 RNA-polymerase promoter allows in vitro transcription from the PCR products, generating RNA that in the presence of reverse transcriptase and modified nucleotides generates fluorescently labeled cDNA. The fluorescently labeled cDNA is then used in subsequent microarray hybridizations.

Found at doi:10.1371/journal.pgen.0030154.sg001 (22 KB PDF).

Figure S2. Rank Distribution of *E. coli* Essential Genes Based on the Hybridization Intensities of the Unselected Library of Mutants

Genes were ranked in ascending order according to the hybridization intensities of the unselected library. Essential genes were obtained from the literature [79] and were graphed based on their rank in the hybridizations of the unselected library. Of the 303 essential genes identified by Baba et al. [79], 263 were present on the array and are represented in the histogram. The histogram was generated by placing the gene ranks in a non-overlapping sliding window of 100 genes. Outliers may be due to strain-specific differences, since the strain used in [79] was *E. coli* W3110 and the strain used in this study was *E. coli* MG1655. As can be seen in this histogram, nearly all essential genes rank in the bottom 15% of hybridization values, thereby providing strong statistical support for our method of genetic functional analysis.

Found at doi:10.1371/journal.pgen.0030154.sg002 (24 KB PDF).

Figure S3. Fraction of Nonmotile Mutants at Each Stage of Enrichment

(A) To estimate the fraction of mutants that are nonmotile during enrichment, cells at the site of inoculation were extracted from the agar, diluted, and plated to obtain individual colonies. Fifty colonies were sampled at random and cultured, and 1 μl of each culture was stabbed into semi-solid agar.
(B–F) The fraction of nonmotile mutants at each stage of enrichment was determined by evaluating motility of fifty mutants picked at random. Semi-solid plates containing motile mutants are highlighted with green boxes and semi-solid plates containing nonmotile mutants are highlighted with red boxes.
(G) The graphical illustration shows a dramatic increase in the percentage of nonmotile mutants during the enrichment procedure.

Found at doi:10.1371/journal.pgen.0030154.sg003 (2.7 MB PDF).

Figure S4. Mutants Resistant to Infection by Bacteriophage χ

Swimming motility assays on a sample of mutants at the end of selection revealed that 98% are defective in motility. Nonmotile mutants are highlighted with red frames and the single motile mutant is shown with a green frame.

Found at doi:10.1371/journal.pgen.0030154.sg004 (487 KB PDF).

Figure S5. Determining Percentage of Nonswarming Mutants after Enrichment

Swarming assays on a sample of mutants at the end of selection revealed >90% to show either an absolute or quantitative defect in swarming. Images in red frames indicate nonswarming mutants and the single image in the green frame represents a mutant capable of swarming.

Found at doi:10.1371/journal.pgen.0030154.sg005 (515 KB PDF).

Figure S6. Representative Images of LPS and OPG Mutants

Images to the left of the electron micrographs are soft-agar swim plates and the images to the right of the micrographs are of swarming plates. The four columns to the far left of the figure are of wild-type and Δ*cpsB* mutant strains that were transformed with empty pBAD18 or with pBAD18 carrying the *flhDC* operon cloned in front of the arabinose-inducible promoter. The *cpsB* gene was targeted for deletion because it has been found to be among the genes responsible for capsular polysaccharide colanic acid synthesis [80], whose expression gives LPS mutants their mucoid phenotype [37]. Overnight cultures were used to inoculate these soft-agar plates containing 100 μg/ml ampicillin and 0.2% arabinose. Images were taken after 8 h at 30 °C. The results indicate that motility of LPS and OPG mutants can be enhanced by expressing *flhDC* from plasmid DNA. Furthermore, LPS mutants with the Δ*cpsB* deletion show greater motility in soft-agar plates, indicating that capsule synthesis is partly responsible for the observed motility defect. The four columns in the center are double mutants corresponding to the column and row headings. The results suggest that disrupting the Rcs signaling pathway in LPS and OPG mutants rescue swimming motility by preventing repression of the *flhDC* operon and reducing activation of the *cps* operon. This conclusion is partly supported by the observed increase in flagella in the electron micrographs (columns 9 and 10) for some of the mutants with severely impaired motility (*gmhA*, *hldD*, and *rfaB*) when a Δ*rcsF* double mutation is introduced. The two columns to the far right of the figure contain images of swarm plates; the results are a subset of the images in Figure 3 and show that disrupting Rcs signaling rescues the swarming defect of LPS and OPG single mutants. Deletion mutants were created using the method by Datsenko and Wanner [81]. Electron micrographs and swarming assays were prepared as described in Protocol S2 and Materials and Methods, respectively. Bars, 1 μm.

Found at doi:10.1371/journal.pgen.0030154.sg006 (1.4 MB PDF).

Figure S7. Reduction in Motility Exhibited by *rcsC137*

Soft agar was inoculated with wild-type and *rcsC137* strains. Images were taken after an 8-h incubation at 30 °C.

Found at doi:10.1371/journal.pgen.0030154.sg007 (152 KB PDF).

Figure S8. Suppressor Mutations of the Δ*hns* Motility Defect

(A) Suppressor mutations of the motility defect were identified by inoculating soft-agar plates with the Δ*hns* mutant (left) and the Δ*hns* double mutants (right). Mutants in which the motility defect was suppressed were extracted from the agar (bracketed with a red dashed line) and used for further analyses.
(B) Among the 14 suppressor mutations sampled from the Δ*hns* background, ten were insertions in *clpX* and four were found within *clpP* (Table S3). These genes encode the ClpXP complex, a protease found to degrade FlhDC and thus decrease expression of class 2 and class 3 flagellar operons [82]. These results suggest that insertions in *clpX* and *clpP* increase stability of FlhDC and function to counteract the impaired motility due to reduced *flhDC* expression observed in an *hns* mutant. To test this possibility, we introduced *flhDC-lacZ* translational fusions and performed β-galactosidase assays in strains in which a deletion of hns is combined with insertions in *clpX* or *clpP*. We found that mutations in both *clpX* and *clpP* increase the levels of FlhDC compared to an *hns*-single mutant (unpublished data). Microarray hybridization of the PCR products generated from the mutants extracted from the motile front guided the identification of four additional genes whose insertional mutagenesis partly suppress the motility defect of the Δ*hns* mutant: *rcsB*, *hdfR*, *yicC*, and *yobF*. Mutations in *hdfR* had been previously shown to rescue motility in the *hns* mutant background [83]. The identification of *rcsB* as a suppressor suggests that under these conditions, the RcsB transcription factor is mildly repressing *flhDC* expression and that its disruption partially derepresses *flhDC*, and, in turn, enhances motility. Follow-up work is currently underway to determine the mechanistic basis of suppression by *yicC* and *yobF* mutations.
(C) Model illustrating cellular components that, when mutated, suppress the motility defect of the Δ*hns* strain. Novel interactions are denoted by red dotted arrows and confirmed known interactions are denoted by blue dotted arrows.

Found at doi:10.1371/journal.pgen.0030154.sg008 (279 KB PDF).

Figure S9. Effects of *yfgF* and *yfgG* Deletions in the Δ*yhjH* Background

Deletions of *yfgF* and *yfgG* do not suppress the motility defect of the Δ*yhjH* mutant.

Found at doi:10.1371/journal.pgen.0030154.sg009 (207 KB PDF).

Figure S10. Multiple-Sequence Alignment of EAL Domains of YfgF and YegE with Enzymatically Active EAL Domains

The multiple-sequence alignment of enzymatically active EAL domains [84] with the EAL domains of YfgF and YegE was created using CLUSTAL-W [85]. The namesake amino-acid motif for this protein domain family, EAL, is indicated by red background and a conserved motif (DDFGTG) hypothesized to be essential for PDE activity [84] is indicated by a blue background. Residues conserved in each of the enzymatically active domains are represented by an asterisk. Residues conserved in >80% of the active domains are indicated by black background. Residues sharing common classifications—nonpolar, uncharged polar, or charged polar R groups—present in >80% of the active domains are indicated by gray background.

Found at doi:10.1371/journal.pgen.0030154.sg010 (57 KB PDF).

Figure S11. Behavior of Mutants Expressing Fimbriae

Phase OFF and Phase ON mutants are *fimB fimE* double mutants. Phase ON mutants have the invertible element oriented to direct transcription of the *fimA* operon (on) whereas phase OFF mutants contain the element in the alternate orientation (off). *fimS* mutants contain a transposon insertion within the invertible element, thereby locking it in the "ON" orientation.
(A) Transmission electron micrographs. Bars, 1 μm.
(B) Soft agar swim plates.
(C) Swarming assays on Eiken agar.
(D) Distribution of flagella on WT, "ON," "OFF," and *fimS*::Tn5 cells. Transmission electron micrographs were taken and the flagella were counted on 75 cells chosen at random from each strain.

Found at doi:10.1371/journal.pgen.0030154.sg011 (1.1 MB PDF).

Figure S12. Genetic Basis of Motility Repression by High-Salt Conditions

(A) The transposon mutant library was added to the tryptone agar containing 500 mM NaCl. After an incubation at 30 °C for 32 h, the mutants were extracted from the area of the agar indicated by the dashed red line, lysed, and the DNA was manipulated as described in the Materials and Methods.
(B) The *znuA* and *envZ* transcriptional units are shown. Seven insertional mutations were mapped to five different locations in the *znuA* gene and one insertion was mapped in *envZ*. Triangles denote the sites of the insertions; strain names appear next to each insertion site.
(C) Motility of WT *E. coli* was assayed in 100 mM and 500 mM NaCl at 30 °C for 8 h.
(D) Mutants identified in high salt show a dramatic increase in motility relative to the wild-type strain in tryptone soft agar with 500 mM NaCl. Images were taken after 12 h of incubation at 30 °C.
(E) Model illustrating cellular components found to influence motility in high-salt conditions.

Found at doi:10.1371/journal.pgen.0030154.sg012 (439 KB PDF).

Movie S1. Time Lapse of Swarming Wild-Type *E. coli*

Cells are expressing green fluorescent protein and are viewed using confocal microscopy.

Found at doi:10.1371/journal.pgen.0030154.sv001 (6.1 MB WMV).

Protocol S1. Microarray Construction and Hybridization

Found at doi:10.1371/journal.pgen.0030154.sd014 (35 KB DOC).

Protocol S2. Molecular Techniques and Microscopy

Found at doi:10.1371/journal.pgen.0030154.sd015 (27 KB DOC).

Table S1. Non-flagellar Genes Affecting Motility Identified in Swimming, Swarming, and Bacteriophage χ Selections

Found at doi:10.1371/journal.pgen.0030154.st001 (31 KB DOC).

Table S2. Array of *z*-Scores for the 29 *E. coli* Genes Containing GGDEF and/or EAL Domains after Enrichment for Nonswimming and Nonswarming Mutants and after the Genome-Wide Selection for Δ*yhjH* Motility

Found at doi:10.1371/journal.pgen.0030154.st002 (32 KB DOC).

Table S3. *E. coli* Strains

Found at doi:10.1371/journal.pgen.0030154.st003 (231 KB DOC).

Table S4. Bacteriophage and Plasmids Used in This Study

Found at doi:10.1371/journal.pgen.0030154.st004 (26 KB DOC).

Table S5. Oligonucleotides

Found at doi:10.1371/journal.pgen.0030154.st005 (86 KB DOC).

Acknowledgments

We thank the members of the Tavazoie laboratory for helpful discussions. We are grateful to Margaret Bisher for assisting with the electron microscopy. We thank Makoto Miyata for the gift of Eiken agar.

Author contributions. HSG and ST conceived and designed the experiments and wrote the paper. HSG performed the experiments. HSG, YL, and ST analyzed the data. YL and WSR contributed reagents/materials/analysis tools.

Funding. WSR is a Lewis-Sigler Fellow. ST is supported in part by grants from the National Science Foundation and the National Institutes of Health.

Competing interests. The authors have declared that no competing interests exist.

References

1. Rusch DB, Halpern AL, Sutton G, Heidelberg KB, Williamson S, et al. (2007) The Sorcerer II global ocean sampling expedition: Northwest Atlantic through eastern tropical Pacific. PLoS Biol 5: e77. doi:10.1371/journal.pbio.0050077
2. Berg HC (2003) The rotary motor of bacterial flagella. Annu Rev Biochem 72: 19–54.
3. Macnab RM (2003) How bacteria assemble flagella. Annu Rev Microbiol 57: 77–100.
4. Wadhams GH, Armitage JP (2004) Making sense of it all: Bacterial chemotaxis. Nat Rev Mol Cell Biol 5: 1024–1037.
5. Macnab RM (1996) Flagella and motility. In: Neidhardt FC, Curtiss R, Ingraham JL, Lin ECC, Low KB, et al., editors. *Escherichia coli* and *Salmonella:* Cellular and molecular biology. 2nd ed. Washington (District of Columbia): American Society for Microbiology Press. pp. 123–145.
6. Stock JB, Surette MG (1996) Chemotaxis. In: Neidhardt FC, Curtiss R, Ingraham JL, Lin ECC, Low KB, et al., editors. *Escherichia coli* and *Salmonella:* Cellular and molecular biology. 2nd ed. Washington (District of Columbia): American Society for Microbiology Press. 1103–1129.
7. Alon U, Surette MG, Barkai N, Leibler S (1999) Robustness in bacterial chemotaxis. Nature 397: 168–171.
8. Sourjik V (2004) Receptor clustering and signal processing in *E. coli* chemotaxis. Trends Microbiol 12: 569–576.
9. Berg HC (1993) Random walks in biology. Princeton (New Jersey): Princeton University Press. 152 p.
10. Kalir S, McClure J, Pabbaraju K, Southward C, Ronen M, et al. (2001) Ordering genes in a flagella pathway by analysis of expression kinetics from living bacteria. Science 292: 2080–2083.
11. Zaslaver A, Mayo AE, Rosenberg R, Bashkin P, Sberro H, et al. (2004) Just-in-time transcription program in metabolic pathways. Nat Genet 36: 486–491.
12. Badarinarayana V, Estep PW 3rd, Shendure J, Edwards J, Tavazoie S, et al. (2001) Selection analyses of insertional mutants using subgenic-resolution arrays. Nat Biotechnol 19: 1060–1065.
13. Smith V, Botstein D, Brown PO (1995) Genetic footprinting: A genomic strategy for determining a gene's function given its sequence. Proc Natl Acad Sci U S A 92: 6479–6483.
14. Schena M, Shalon D, Davis RW, Brown PO (1995) Quantitative monitoring of gene expression patterns with a complementary DNA microarray. Science 270: 467–470.
15. Hayes F (2003) Transposon-based strategies for microbial functional genomics and proteomics. Annu Rev Genet 37: 3–29.
16. Reznikoff WS, Goryshin IY, Jendrisak JJ (2004) Tn5 as a molecular genetics tool: In vitro transposition and the coupling of in vitro technologies with in vivo transposition. In: Miller WJ, Capy P, editors. Mobile genetic elements: Protocols and genomic applications. Totowa (New Jersey): Humana Press. pp. 83–96.
17. Adler J (1966) Chemotaxis in bacteria. Science 153: 708–716.
18. Berg HC (2004) *E. coli* in motion. New York: Springer–Verlag. 133 p.
19. Yokoseki T, Iino T, Kutsukake K (1996) Negative regulation by *fliD, fliS,* and *fliT* of the export of the flagellum-specific anti-sigma factor, FlgM, in *Salmonella typhimurium.* J Bacteriol 178: 899–901.
20. Kutsukake K, Ikebe T, Yamamoto S (1999) Two novel regulatory genes, *fliT* and *fliZ,* in the flagellar regulon of *Salmonella.* Genes Genet Syst 74: 287–292.
21. Yamamoto S, Kutsukake K (2006) FliT acts as an anti-$FlhD_2C_2$ factor in the transcriptional control of the flagellar regulon in *Salmonella enterica* serovar typhimurium. J Bacteriol 188: 6703–6708.
22. Rebbapragada A, Johnson MS, Harding GP, Zuccarelli AJ, Fletcher HM, et al. (1997) The Aer protein and the serine chemoreceptor Tsr independently sense intracellular energy levels and transduce oxygen, redox, and energy signals for *Escherichia coli* behavior. Proc Natl Acad Sci U S A 94: 10541–10546.
23. Hazelbauer GL, Harayama S (1979) Mutants in transmission of chemotactic signals from two independent receptors of *E. coli.* Cell 16: 617–625.
24. Schade SZ, Adler J, Ris H (1967) How bacteriophage χ attacks motile bacteria. J Virol 1: 599–609.
25. Samuel AD, Pitta TP, Ryu WS, Danese PN, Leung EC, et al. (1999) Flagellar determinants of bacterial sensitivity to χ-phage. Proc Natl Acad Sci U S A 96: 9863–9866.
26. Hess JF, Oosawa K, Kaplan N, Simon MI (1988) Phosphorylation of three proteins in the signaling pathway of bacterial chemotaxis. Cell 53: 79–87.
27. Welch M, Oosawa K, Aizawa S, Eisenbach M (1993) Phosphorylation-dependent binding of a signal molecule to the flagellar switch of bacteria. Proc Natl Acad Sci U S A 90: 8787–8791.
28. Harshey RM (1994) Bees aren't the only ones: Swarming in gram-negative bacteria. Mol Microbiol 13: 389–394.

29. Harshey RM, Matsuyama T (1994) Dimorphic transition in *Escherichia coli* and *Salmonella typhimurium*: Surface-induced differentiation into hyperflagellate swarmer cells. Proc Natl Acad Sci U S A 91: 8631–8635.
30. Wang Q, Suzuki A, Mariconda S, Porwollik S, Harshey RM (2005) Sensing wetness: A new role for the bacterial flagellum. Embo J 24: 2034–2042.
31. Mariconda S, Wang Q, Harshey RM (2006) A mechanical role for the chemotaxis system in swarming motility. Mol Microbiol 60: 1590–1602.
32. Fiedler W, Rotering H (1988) Properties of *Escherichia coli* mutants lacking membrane-derived oligosaccharides. J Biol Chem 263: 14684–14689.
33. Oshima T, Aiba H, Masuda Y, Kanaya S, Sugiura M, et al. (2002) Transcriptome analysis of all two-component regulatory system mutants of *Escherichia coli* K-12. Mol Microbiol 46: 281–291.
34. Ebel W, Vaughn GJ, Peters HK 3rd, Trempy JE (1997) Inactivation of *mdoH* leads to increased expression of colanic acid capsular polysaccharide in *Escherichia coli*. J Bacteriol 179: 6858–6861.
35. Parker CT, Kloser AW, Schnaitman CA, Stein MA, Gottesman S, et al. (1992) Role of the *rfaG* and *rfaP* genes in determining the lipopolysaccharide core structure and cell surface properties of *Escherichia coli* K-12. J Bacteriol 174: 2525–2538.
36. Francez-Charlot A, Laugel B, Van Gemert A, Dubarry N, Wiorowski F, et al. (2003) RcsCDB His-Asp phosphorelay system negatively regulates the *flhDC* operon in *Escherichia coli*. Mol Microbiol 49: 823–832.
37. Majdalani N, Gottesman S (2005) The Rcs phosphorelay: A complex signal transduction system. Annu Rev Microbiol 59: 379–405.
38. Majdalani N, Heck M, Stout V, Gottesman S (2005) Role of RcsF in signaling to the Rcs phosphorelay pathway in *Escherichia coli*. J Bacteriol 187: 6770–6778.
39. Majdalani N, Hernandez D, Gottesman S (2002) Regulation and mode of action of the second small RNA activator of RpoS translation, RprA. Mol Microbiol 46: 813–826.
40. Brill JA, Quinlan-Walshe C, Gottesman S (1988) Fine-structure mapping and identification of two regulators of capsule synthesis in *Escherichia coli* K-12. J Bacteriol 170: 2599–2611.
41. Toguchi A, Siano M, Burkart M, Harshey RM (2000) Genetics of swarming motility in *Salmonella enterica* serovar typhimurium: Critical role for lipopolysaccharide. J Bacteriol 182: 6308–6321.
42. Frye J, Karlinsey JE, Felise HR, Marzolf B, Dowidar N, et al. (2006) Identification of new flagellar genes of *Salmonella enterica* serovar Typhimurium. J Bacteriol 188: 2233–2243.
43. Parkinson JS (1977) Behavioral genetics in bacteria. Annu Rev Genet 11: 397–414.
44. Block SM, Segall JE, Berg HC (1982) Impulse responses in bacterial chemotaxis. Cell 31: 215–226.
45. Eisenbach M, Caplan SR (1998) Bacterial chemotaxis: Unsolved mystery of the flagellar switch. Curr Biol 8: R444–R446.
46. Collins SR, Miller KM, Maas NL, Roguev A, Fillingham J, et al. (2007) Functional dissection of protein complexes involved in yeast chromosome biology using a genetic interaction map. Nature 446: 806–810.
47. Tong AH, Lesage G, Bader GD, Ding H, Xu H, et al. (2004) Global mapping of the yeast genetic interaction network. Science 303: 808–813.
48. Ryjenkov DA, Simm R, Römling U, Gomelsky M (2006) The PilZ domain is a receptor for the second messenger c-di-GMP: The PilZ domain protein YcgR controls motility in enterobacteria. J Biol Chem 281: 30310–30314.
49. Römling U, Gomelsky M, Galperin MY (2005) C-di-GMP: The dawning of a novel bacterial signalling system. Mol Microbiol 57: 629–639.
50. Ryjenkov DA, Tarutina M, Moskvin OV, Gomelsky M (2005) Cyclic diguanylate is a ubiquitous signaling molecule in bacteria: Insights into biochemistry of the GGDEF protein domain. J Bacteriol 187: 1792–1798.
51. Tamayo R, Tischler AD, Camilli A (2005) The EAL domain protein VieA is a cyclic diguanylate phosphodiesterase. J Biol Chem 280: 33324–33330.
52. Simm R, Morr M, Kader A, Nimtz M, Römling U (2004) GGDEF and EAL domains inversely regulate cyclic di-GMP levels and transition from sessility to motility. Mol Microbiol 53: 1123–1134.
53. Christen M, Christen B, Folcher M, Schauerte A, Jenal U (2005) Identification and characterization of a cyclic di-GMP-specific phosphodiesterase and its allosteric control by GTP. J Biol Chem 280: 30829–30837.
54. Tal R, Wong HC, Calhoon R, Gelfand D, Fear AL, et al. (1998) Three *cdg* operons control cellular turnover of cyclic di-GMP in *Acetobacter xylinum:* Genetic organization and occurrence of conserved domains in isoenzymes. J Bacteriol 180: 4416–4425.
55. Galperin MY, Nikolskaya AN, Koonin EV (2001) Novel domains of the prokaryotic two-component signal transduction systems. FEMS Microbiol Lett 203: 11–21.
56. Jenal U, Malone J (2006) Mechanisms of cyclic-di-GMP signaling in bacteria. Annu Rev Genet 40: 385–407.
57. Römling U, Amikam D (2006) Cyclic di-GMP as a second messenger. Curr Opin Microbiol 9: 218–228.
58. Kader A, Simm R, Gerstel U, Morr M, Römling U (2006) Hierarchical involvement of various GGDEF domain proteins in rdar morphotype development of *Salmonella enterica* serovar Typhimurium. Mol Microbiol 60: 602–616.
59. Weber H, Pesavento C, Possling A, Tischendorf G, Hengge R (2006) Cyclic-di-GMP-mediated signalling within the sigma network of *Escherichia coli*. Mol Microbiol 62: 1014–1034.
60. Klemm P (1986) Two regulatory *fim* genes, *fimB* and *fimE,* control the phase variation of type 1 fimbriae in *Escherichia coli*. EMBO J 5: 1389–1393.
61. Abraham JM, Freitag CS, Clements JR, Eisenstein BI (1985) An invertible element of DNA controls phase variation of type 1 fimbriae of *Escherichia coli*. Proc Natl Acad Sci USA 82: 5724–5727.
62. Adler J, Templeton B (1967) The effect of environmental conditions on the motility of *Escherichia coli*. J Gen Microbiol 46: 175–184.
63. Li C, Louise CJ, Shi W, Adler J (1993) Adverse conditions which cause lack of flagella in *Escherichia coli*. J Bacteriol 175: 2229–2235.
64. Morrison RB, McCapra J (1961) Flagellar changes in *Escherichia coli* induced by temperature of the environment. Nature 192: 774–776.
65. Soutourina OA, Bertin PN (2003) Regulation cascade of flagellar expression in Gram-negative bacteria. FEMS Microbiol Rev 27: 505–523.
66. Shin S, Park C (1995) Modulation of flagellar expression in *Escherichia coli* by acetyl phosphate and the osmoregulator OmpR. J Bacteriol 177: 4696–4702.
67. Russo FD, Silhavy TJ (1991) EnvZ controls the concentration of phosphorylated OmpR to mediate osmoregulation of the porin genes. J Mol Biol 222: 567–580.
68. Margulies M, Egholm M, Altman WE, Attiya S, Bader JS, et al. (2005) Genome sequencing in microfabricated high-density picolitre reactors. Nature 437: 376–380.
69. Shendure J, Porreca GJ, Reppas NB, Lin X, McCutcheon JP, et al. (2005) Accurate multiplex polony sequencing of an evolved bacterial genome. Science 309: 1728–1732.
70. Chan K, Kim CC, Falkow S (2005) Microarray-based detection of *Salmonella enterica* serovar Typhimurium transposon mutants that cannot survive in macrophages and mice. Infect Immun 73: 5438–5449.
71. Lawley TD, Chan K, Thompson LJ, Kim CC, Govoni GR, et al. (2006) Genome-wide screen for *Salmonella* genes required for long-term systemic infection of the mouse. PLoS Pathog 2: e11. doi:10.1371/journal.ppat.0020011
72. Rengarajan J, Bloom BR, Rubin EJ (2005) Genome-wide requirements for *Mycobacterium tuberculosis* adaptation and survival in macrophages. Proc Natl Acad Sci U S A 102: 8327–8332.
73. Sassetti CM, Boyd DH, Rubin EJ (2003) Genes required for mycobacterial growth defined by high density mutagenesis. Mol Microbiol 48: 77–84.
74. Stewart GR, Patel J, Robertson BD, Rae A, Young DB (2005) Mycobacterial mutants with defective control of phagosomal acidification. PLoS Pathog 1: e33. doi:10.1371/journal.ppat.0010033
75. Blattner FR, Plunkett G 3rd, Bloch CA, Perna NT, Burland V, et al. (1997) The complete genome sequence of *Escherichia coli* K-12. Science 277: 1453–1474.
76. Silhavy TJ, Berman ML, Enquist LW (1984) Experiments with gene fusions. Plainview (New York): Cold Spring Harbor Press. 303 p.
77. Slauch JM, Silhavy TJ (1991) *cis*-acting *ompF* mutations that result in OmpR-dependent constitutive expression. J Bacteriol 173: 4039–4048.
78. Tavazoie S, Church GM (1998) Quantitative whole-genome analysis of DNA-protein interactions by in vivo methylase protection in *E. coli*. Nat Biotechnol 16: 566–571.
79. Baba T, Ara T, Hasegawa M, Takai Y, Okumura Y, et al. (2006) Construction of *Escherichia coli* K-12 in-frame, single-gene knockout mutants: The Keio collection. Mol Syst Biol 2: 2006.0008.
80. Trisler P, Gottesman S (1984) *lon* transcriptional regulation of genes necessary for capsular polysaccharide synthesis in *Escherichia coli* K-12. J Bacteriol 160: 184–191.
81. Datsenko KA, Wanner BL (2000) One-step inactivation of chromosomal genes in *Escherichia coli* K-12 using PCR products. Proc Natl Acad Sci U S A 97: 6640–6645.
82. Tomoyasu T, Takaya A, Isogai E, Yamamoto T (2003) Turnover of FlhD and FlhC, master regulator proteins for *Salmonella* flagellum biogenesis, by the ATP-dependent ClpXP protease. Mol Microbiol 48: 443–452.
83. Ko M, Park C (2000) Two novel flagellar components and H-NS are involved in the motor function of *Escherichia coli*. J Mol Biol 303: 371–382.
84. Schmidt AJ, Ryjenkov DA, Gomelsky M (2005) The ubiquitous protein domain EAL is a cyclic diguanylate-specific phosphodiesterase: enzymatically active and inactive EAL domains. J Bacteriol 187: 4774–4781.
85. Thompson JD, Higgins DG, Gibson TJ (1994) CLUSTAL W: Improving the sensitivity of progressive multiple sequence alignment through sequence weighting, position-specific gap penalties and weight matrix choice. Nucleic Acids Res 22: 4673–4680.
86. Taylor BL, Zhulin IB (1999) PAS domains: Internal sensors of oxygen, redox potential, and light. Microbiol Mol Biol Rev 63: 479–506.
87. Nikolskaya AN, Mulkidjanian AY, Beech IB, Galperin MY (2003) MASE1 and MASE2: Two novel integral membrane sensory domains. J Mol Microbiol Biotechnol 5: 11–16.